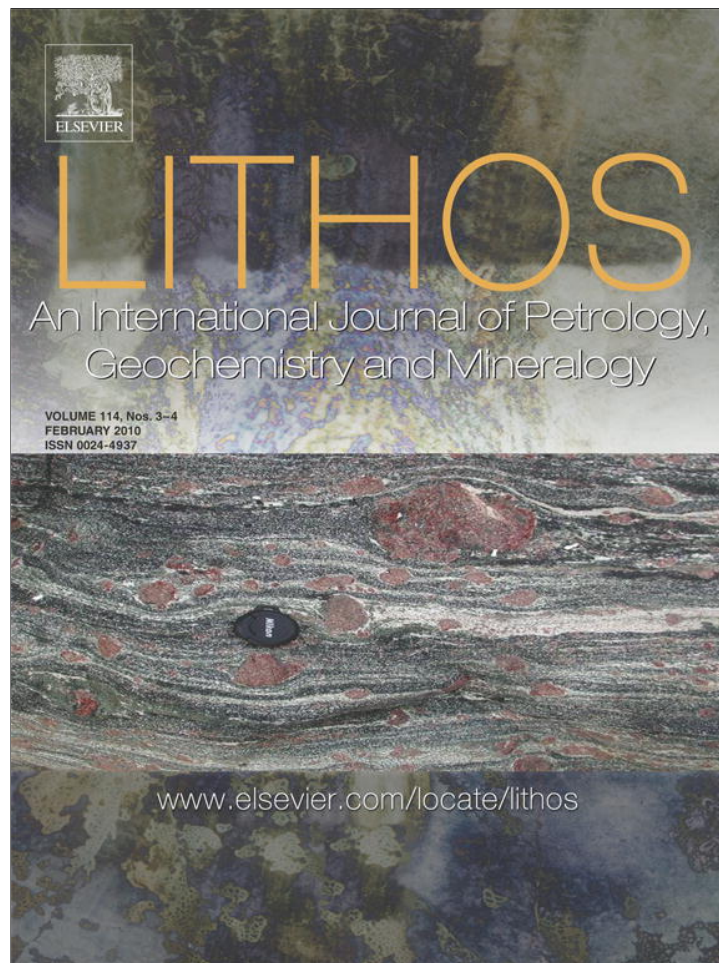


Provided for non-commercial research and education use.
Not for reproduction, distribution or commercial use.



This article appeared in a journal published by Elsevier. The attached copy is furnished to the author for internal non-commercial research and education use, including for instruction at the authors institution and sharing with colleagues.

Other uses, including reproduction and distribution, or selling or licensing copies, or posting to personal, institutional or third party websites are prohibited.

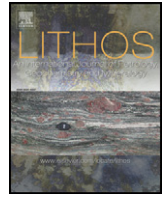
In most cases authors are permitted to post their version of the article (e.g. in Word or Tex form) to their personal website or institutional repository. Authors requiring further information regarding Elsevier's archiving and manuscript policies are encouraged to visit:

<http://www.elsevier.com/copyright>



Contents lists available at ScienceDirect

Lithos

journal homepage: www.elsevier.com/locate/lithos

Corundum-bearing garnet peridotite from northern Dominican Republic: A metamorphic product of an arc cumulate in the Caribbean subduction zone

Kéiko H. Hattori ^{a,*}, Stéphane Guillot ^b, Benoit-Michel Saumur ^{a,1}, Mike N. Tubrett ^c, Olivier Vidal ^b, Samuel Morfin ^{b,2}

^a Department of Earth Sciences, University of Ottawa, Ottawa, Ontario, Canada K1N 6N5

^b Laboratoire de Géodynamique des Chaînes Alpines, Centre National de la Recherche Scientifique, University of Grenoble, 1381 rue de la Piscine, 38041, Grenoble, France

^c Inco Innovation Centre, Memorial University of Newfoundland, St. John's, Newfoundland, Canada

ARTICLE INFO

Article history:

Received 18 June 2009

Accepted 7 October 2009

Available online 21 October 2009

Keywords:

Garnet peridotite

Mantle flow

Arc cumulates

Subduction channel

Corundum

Ultra-high pressure metamorphism

Caribbean arc

ABSTRACT

Garnet peridotite in oceanic subduction complexes has been reported only in two locations in the world. One of these examples occurs in the late Cretaceous to early Tertiary subduction complex in northern Dominican Republic. The garnet peridotite (wehrlite and olivine-bearing clinopyroxenite) occurs as large (≤ 4 m) boulders together with boulders of eclogites and serpentinites along a narrow (< 10 m) stream of the Rio Cuavas in the southern part of the Rio San Juan Complex. The peridotite is composed of garnet, diopsidic clinopyroxene (partially altered to magnesiohornblende), olivine (extensively altered to serpentine), Al-spinel and minor corundum; the latter two are mostly enclosed in garnet. Coarse-grained garnet also encloses small grains of early-formed garnet that contain Ca- and Al-rich cores and Mg-rich rims.

The garnet peridotite contains low Cr, Ni, and Ir-group platinum group elements in bulk rock compared to primitive mantle values, low Mg (Mg#; 0.74–0.83) and NiO (< 0.1 wt.%) in olivine, and elevated concentrations of fluid-mobile elements (Sr, Pb and U) in clinopyroxene and bulk rock. Combined with the rare earth element data of bulk rocks and clinopyroxene, these data suggest that the peridotite originally solidified as a plagioclase-bearing cumulate of an arc melt at a shallow depth, < 35 km, in the mantle wedge. The cumulate was later dragged by mantle flow from the subarc mantle towards the subduction plane. Subsequent downward movement along the subduction plane resulted in the crystallization of corundum and Ca- and Al-rich garnet at the expense of plagioclase, at a depth of ~ 50 km. The garnet peridotite continued to be subducted to a depth of ~ 120 km, causing a progressive increase in pressure and temperature that resulted in the crystallization of Mg-rich garnet. The garnet peridotite was then exhumed in the serpentinite subduction channel. These events likely took place during the very early stages of the subduction system, where a strong mantle corner flow was likely produced by poor lubrication along the interface between the subducting plate and the overlying Caribbean Plate.

© 2009 Elsevier B.V. All rights reserved.

1. Introduction

Occurrences of garnet peridotite are reported in many continental collision zones, such as in the Western Gneiss Belt of Norway and the Sulu ultra-high pressure (UHP) belt of China (e.g., Brueckner and Medaris, 2000; Zhang et al., 2003), but it is very rare in oceanic subduction zones. So far only two examples have been reported in the interior of an oceanic subduction zone: in the Sanbagawa belt in

southwestern Japan (Enami et al., 2004; Hattori et al., 2009) and in the Rio San Juan Complex of northern Dominican Republic (Abbott et al., 2005, 2006, 2007; Fig. 1a). In both locations, garnet peridotite occurs in close spatial association with eclogites in high grade parts of these metamorphic terranes. Garnet peridotite in the Dominican Republic is unique in containing minor amounts of corundum, Al_2O_3 . Corundum is rare in mafic–ultramafic complexes and reported only from a few locations; the Beni Bousera massif of northern Morocco (Kornprobst et al., 1990), the Ronda massif of southern Spain (Morishita et al., 2001), the Horoman peridotite complex in northern Japan (Morishita and Arai, 2001; Morishita et al., 2007), and Cabo Ortegal Complex in Spain (Girardeau and Ibarguchi, 1991). Corundum in these mafic–ultramafic complexes occurs in mafic layers and lenses, but corundum in the Rio San Juan Complex occurs within peridotite and clinopyroxenite. Therefore, the presence of corundum and garnet makes the peridotite in northern Dominican Republic a rare example of an ultramafic rock in

* Corresponding author. Tel.: +1 613 562 5800x6866; fax: +1 613 562 5192.

E-mail address: khattori@uottawa.ca (K.H. Hattori).

¹ Present address: Department of Geology, University of Toronto, Toronto, Ontario, Canada.

² Present address: Département des sciences de la Terre, Université du Québec à Chicoutimi, Québec, Canada G7H 2B1.

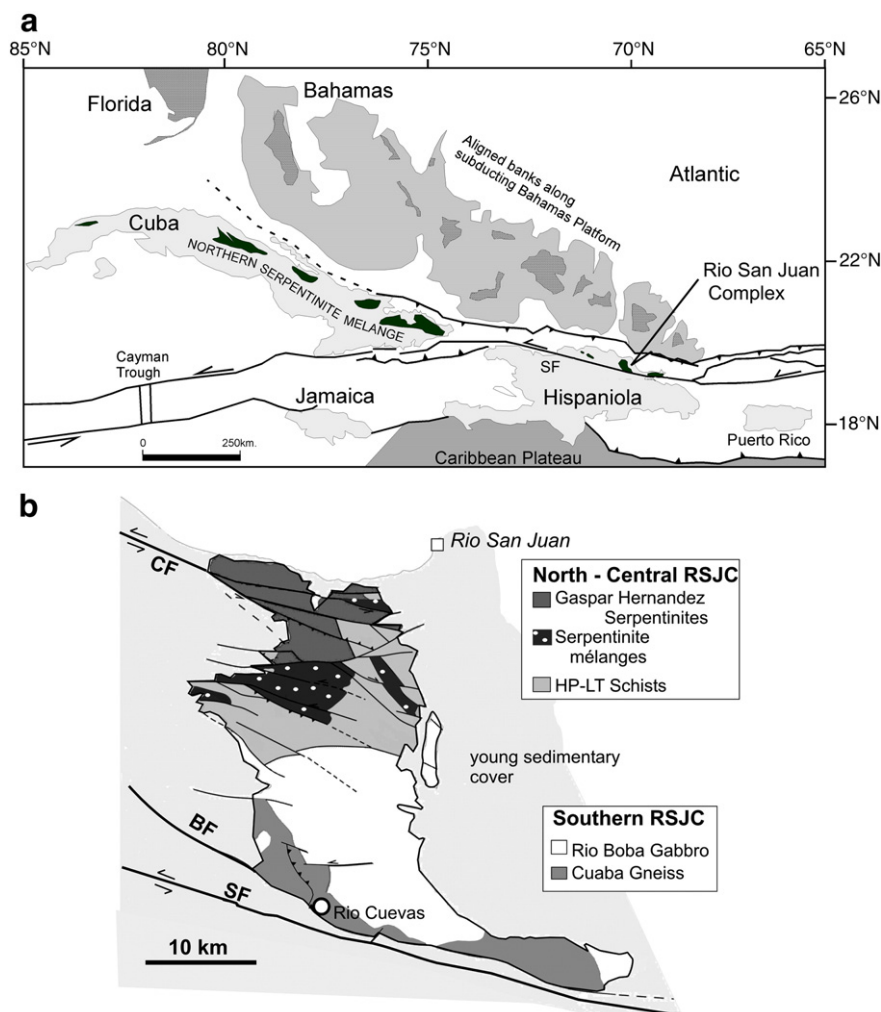


Fig. 1. Location map of the study area. (a) The map is modified after Dolan et al. (1998). The central dark area in the box is shown in panel b. (b) Geological map of the Rio San Juan Complex. BF = Bajabonico fault, CF = Camú fault, SF = Septentrino fault, Map modified from Lewis et al. (1990); Draper and Nagle (1991).

the subduction complex. Thus, this unit may contain information relevant to deep processes in oceanic subduction zones.

Previous study has been conducted on the mineralogy and major element mineral chemistry of the Dominican Republic garnet peridotite (Abbott et al., 2005, 2006, 2007), but the trace elements of the bulk rocks and minerals have not been investigated. Trace element compositions of igneous rocks may provide information relevant to the origin of the parental magmas. This paper presents the compositions of bulk rocks and minerals including the trace element concentrations of clinopyroxene in the corundum- and garnet-bearing peridotites in northern Dominican Republic and discusses their origin.

2. Geological setting

Dominican Republic is in the eastern half of Hispaniola, located on the northern margin of the Caribbean plate (Fig. 1a). Until the Mid to Late Cretaceous, this region was above the NE-dipping Farallon oceanic plate of the Pacific Ocean (Pindell et al., 2005). There was a major change in the plate configuration at ~120 Ma when the subduction complex moved from the Pacific Ocean side to the Atlantic Ocean side, and the North and South American continents diverged (Pindell et al., 2005). The NE move of Hispaniola to its current position was accommodated by a polarity reversal of subduction, and subduction of the Proto-Caribbean oceanic lithosphere below this moving Caribbean plate. This subduction of the Proto-Caribbean oceanic lithosphere produced the Caribbean arc

on the northern margin of the Caribbean plate. The subduction lasted until the middle Eocene, when the oceanic lithosphere was consumed by the subduction and the Caribbean Plate collided with the Bahamas Platform, which is the southern margin of the North American plate (Goncalves et al., 2000; Fig. 1a). This oblique collision produced left-lateral strike-slip faults in northern Hispaniola (Fig. 1), the Septentrional and Camú faults (Goncalves et al., 2000). The strike-slip displacement along the Septentrional fault is greater than 200 km, and is still active with 6 to 12 mm/year strike movement (Prentice et al., 2003).

At present, the northern part of Dominican Republic is mostly covered by young sedimentary rocks ranging in age from late Eocene to Quaternary, and subduction-related rocks are exposed only in isolated stratigraphic windows (or inliers) (Draper and Nagle, 1991; Fig. 1b). The Rio San Juan Complex (~30 × ~30 km), the largest inlier in the area (Fig. 1b), is composed of three juxtaposed parts (Fig. 1b): the Gaspar Hernandez Serpentinities in the northern part, HP metamorphic rocks and tectonic mélanges in the central part, and the Cuaba Gneiss and the Rio Boba Gabbro in the southern part. Garnet peridotite occurs close to the Septentrional fault in the southern extreme of the southern part of the Rio San Juan Complex (Fig. 1b).

The Cuaba Gneiss in the southern part of the Rio San Juan Complex is a metamorphosed oceanic gabbro of the Proto-Caribbean lithosphere (Draper and Nagle, 1991). It is composed of amphibole + quartz + plagioclase ± rutile ± ilmenite ± chlorite ± epidote, and has undergone retrogression under amphibolite facies conditions. The unit, which is well exposed along rivers and on roads, contains

decimetric lenses of eclogites and 100 to 500 m long lonzenges of serpentinites. The eclogite lenses are pervasively hydrated with relict symplectite of plagioclase + diopside + garnet. These lenses are wrapped around by the NW-striking foliation of the Gneiss, suggesting that these eclogites lenses represent less hydrated Cuaba Gneiss, and that the entire unit likely underwent metamorphism under eclogitic conditions.

3. Occurrence of garnet peridotites

The garnet peridotite, which is the focus of this study, occurs along the Rio Cuevas, 10 km NE of the town of San Fransisco de Macoris, in the southern part of the Rio San Juan Complex near the boundary with the Septentrional fault (Fig. 1b). Boulders of garnet peridotite (up to 4 m in size) occur together with boulders of serpentinite (up to 2 m) and eclogites along the narrow (<6 m) and shallow (<50 cm) stream of the Rio Cuevas. The occurrence of garnet peridotite is restricted to a short length (less than 2 km) of the stream that is bordered by hills with dense vegetation. Although outcrops of garnet peridotite were not found due to thick soil cover and vegetation, these boulders are likely derived from proximal sources based on their large size and angular appearance (Fig. 2a), and their restricted occurrence along the stream. Some peridotite boulders show fine layering (~1 cm in width) due to varying abundance of clinopyroxene and olivine and the layering is commonly cut by clinopyroxene veins (up to 1 cm in width; Fig. 2a). The layering is interpreted to be of magmatic origin because the crystals do not show any preferred mineral orientations or other fabrics associated with deformation. The peridotite that does not show layering is also free of any deformation fabrics. The lack of deformation texture is possibly explained by soft serpentinites that might have surrounded garnet peridotite and accommodated strain. Alternatively, high-strain rocks may have been lost during the erosion. The lack of outcrops makes it difficult to assess the validity of these possibilities.

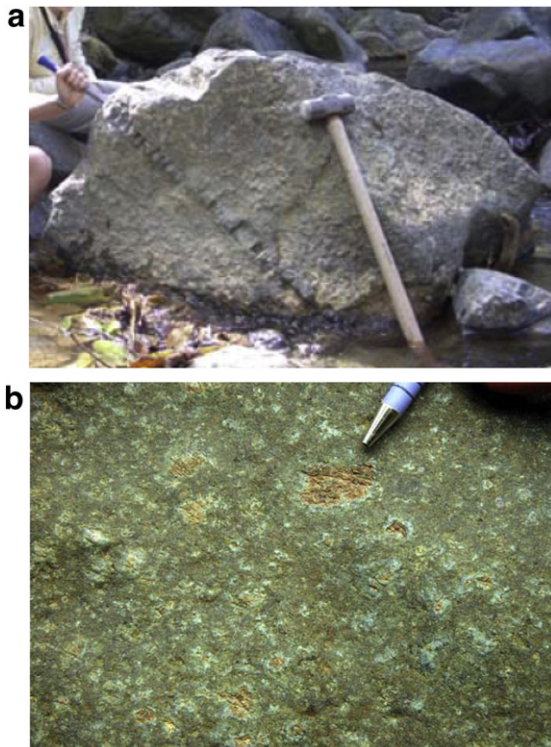


Fig. 2. Photograph of garnet peridotite. (a) Fine grained clinopyroxene-rich vein in garnet wehrlite. (b) Garnet with kelyphitic rim forming a mixture of amphibole and chlorite in garnet wehrlite.

The relationships among three different rock types of boulders along the Rio Cuavas are not certain. Abbott et al. (2005) interpreted the garnet peridotite as part of this Cuaba Gneiss based on their spatial association, but there is no contact between the two rock types. No lenses of garnet peridotite have been observed in the Cuaba Gneiss. The Cuaba Gneiss is considered to be a metamorphosed oceanic gabbro by many workers (e.g., Draper and Nagle, 1991). Recent work by Saumur et al. (2010) showed that the serpentinite in the boulders along the Rio Cuevas originated from the forearc mantle. This evidence suggests that different rock types of boulders in the area may not be genetically associated.

The serpentinite boulders in the stream show similar composition to well-exposed, massive serpentinites near the intersection of the Septentrional and the Bajabonico faults on the property of Lomá Quita Espuela (Fig. 1b). The serpentinites along these major faults are interpreted to have originated from the forearc mantle (Saumur et al., 2010), but we could not find garnet peridotite inclusions in these serpentinite outcrops.

There are also extensive exposures of serpentinite mélanges in the northern and central parts of the Rio San Juan Complex (Fig. 1b). They contain large blocks, >1 m, of blueschists and eclogites, parallel to the foliation of the serpentinite matrix of the mélanges. The matrices of these serpentinite mélanges are interpreted to be hydrated abyssal peridotite based on the mineral chemistry and bulk rock compositions (Saumur et al., 2010). The mélanges are considered to represent the subduction channel that developed during the subduction of the Proto-Caribbean oceanic lithosphere (Krebs et al., 2008; Saumur et al., 2010). These mélanges do not contain fragments of garnet peridotite and may not be directly related to the origin of the garnet peridotite.

4. Lithology of garnet peridotite

Garnet-bearing ultramafic rocks in the area are olivine-bearing clinopyroxenites and wehrlite. Strictly speaking, rocks containing less than 40 vol.% olivine are not peridotite, but the abundance of olivine is close to 40 vol.%. Therefore, these olivine-bearing ultramafic rocks are referred to as garnet peridotite. This nomenclature is also consistent with the rock names used by Abbott et al. (2005). Among different rock types of garnet peridotite, wehrlite with granoblastic garnet is most abundant. Dunite is very rare, but does occur in the same area as the garnet-bearing wehrlite and clinopyroxenites. Although dunite does not contain garnet, it does contain unaltered clinopyroxene (~10 vol.%), unaltered olivine and minor spinel. Since serpentinites spatially associated with garnet peridotite contain no primary silicate minerals and abundant chromite, dunite is distinctly different from serpentinites along the Rio Cuevas. Therefore, the mineral chemistry and bulk rock composition of dunite suggest that dunite belongs to this suite of garnet-bearing peridotites. The lack of garnet and corundum in dunite is likely attributed to low Al in the bulk rock composition.

Garnet peridotite is easily identified in the field, as pink coarse-grained garnet, up to 2.5 cm in size, stands out on the dark surface of boulders (Fig. 2b). Garnet is commonly rimmed by kelyphitic rims (Fig. 2b), which are composed of a mixture of amphibole and chlorite (Fig. 3a). Amphibole has a composition of tremolite and magnesiohornblende. Some grains are totally replaced by kelyphite, but the original garnet grains are outlined by the kelyphite (Fig. 2b).

Serpentine replacing olivine gives a black color to the surface of boulders. Volume expansion during the hydration of olivine results in the formation of serpentine veinlets protruding from the original olivine grains.

4.1. Previous studies of garnet peridotite

This occurrence of garnet-bearing peridotite was first described by Abbott et al. (2005). They reported the mineralogy and major

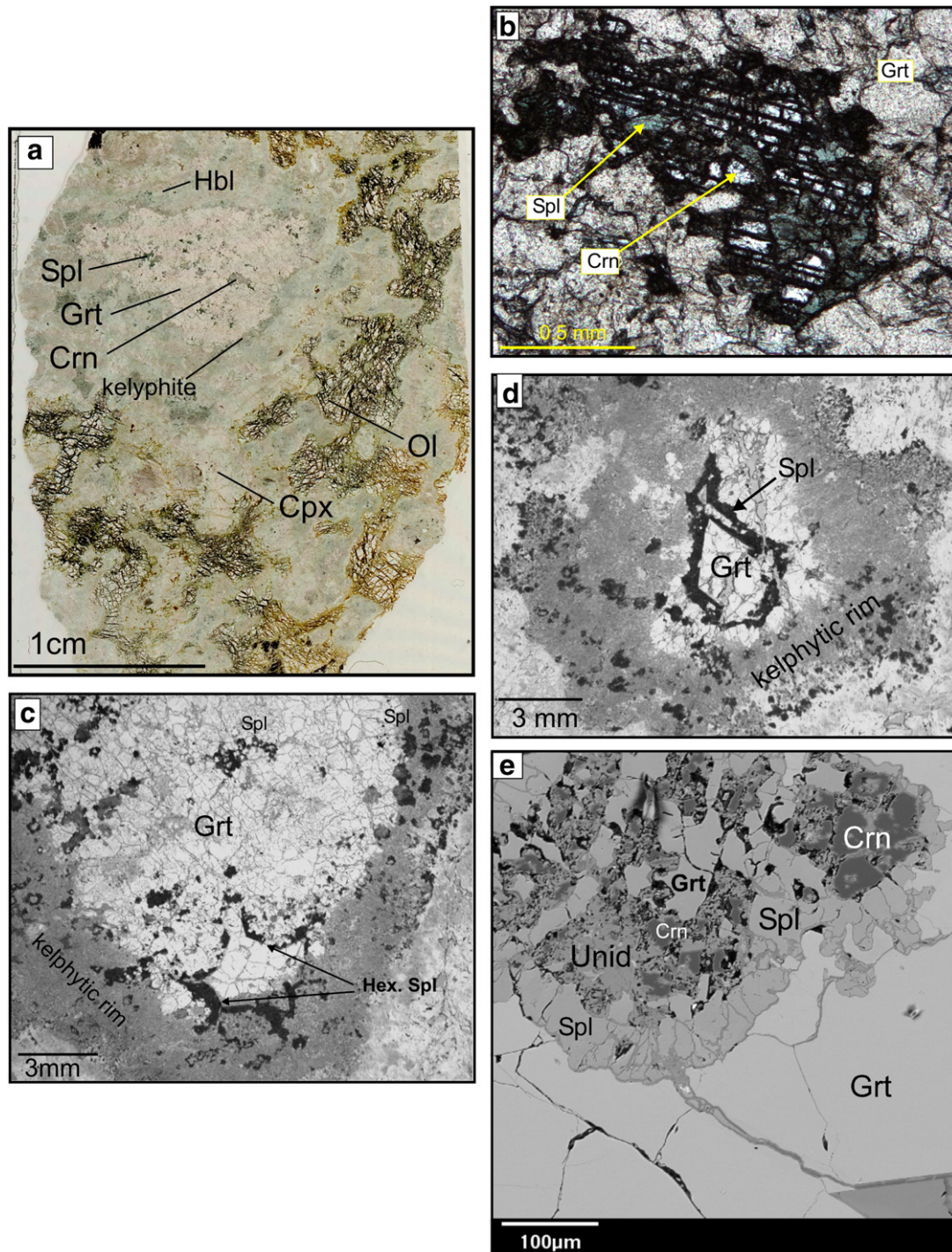


Fig. 3. Corundum and spinel inclusions in garnet. (a) The entire thin section of corundum-bearing garnet peridotite (sample RD 50). Anhedronal garnet (Grt) contains inclusions of Al spinel (Spl) and corundum (Crn) and rimmed by a kelyphite, a mixture of fine-grained hornblende (Hbl) and chlorite. Olivine (Ol) is fractured and filled with serpentine. Diopside clinopyroxene (Cpx) is partially altered to amphibole. (b) Photomicrograph of inclusions in garnet. (c). Photomicrograph of Grt containing hexagonal shaped relict Spl. Note straight outline of the Spl, suggesting that euhedral Spl growth in the former Al mineral, most likely plagioclase. (d) Photomicrograph of skeletal Spl within Grt, showing Grt replaced Spl. (e) Back-scattered electron image of garnet (Grt) containing inclusions of Crn, Spl and unidentified phase (Unid).

element chemistry of representative minerals, and suggested that the rock formed as a cumulate at high T , $> \sim 1600$ °C, and high P , > 34 kbar. Corundum and garnet are all interpreted as magmatic phases. Abbott et al. (2006) suggested that the high P – T cumulate underwent retrogressive metamorphism at 800–850 °C and ~ 30 –40 kbar. Abbott et al. (2007) reaffirmed their earlier interpretation that the garnet peridotite is a cumulate that crystallized under high P – T conditions.

5. Samples

We selected several representative samples for our study (Table 1). There are some low- T secondary minerals, such as amphibole, chlorite, and serpentine, but the hydration is generally not pervasive (Figs. 2b and 3a). The loss on ignition (LOI) values vary from 1 to 3 wt.% in most rocks, except for olivine-rich rocks (7.2 wt.% LOI in RD59 and 4.6 wt.% LOI in RD57). These high LOI values are due to modest

Table 1
The locations and rock types of samples.

	UTM coordinates α		Rock type	Mineralogy (vol. %) β
	Easting	Northing		
RD40	375737	2140179	Crn–Grt–wehrlite	
RD50	375796	2140917	Crn–Grt–wehrlite	Grt (55%) + Ol (35%) + Cpx (30%) + Spl (3%) + Crn
RD51	375796	2140917	Crn–Grt–wehrlite	Grt (50%) + Ol (20%) + Cpx (25%) + Spl + Crn
RD57	375829	2140412	Crn-bearing wehrlite	Ol (75%) + Cpx (20%) + Spl (3%) + Crn
RD59	375905	2140534	dunite	Ol (90%) + Cpx (10%) + Spl (tr)
RD62B	375770	2140644	Crn–Grt–wehrlite	Ol (40%) + Ol (5%) + Cpx (55%) + Spl + Crn
RD63	375708	2140700	Crn–Grt–wehrlite	Grt (40%) + Ol (30%) + Cpx (30%) + Spl + Crn
RD613a	375793	2141105	Crn–Grt–cpxnite	Grt (10%) + Ol (10%) + Cpx (80%) + Spl + Crn
RD613b	375793	2141105	Grt-rich part	Grt (45%) + Ol (20%) + Cpx (30%) + Spl (3%) + Crn

α : UTM coordinates in NAD 27 (Cuba) in Zone 19.

β : Spinel in most samples are Al-rich green spinel excluding spinel grains in dunite (RD59), which contains very minor Cr-spinel that has been altered Cr-bearing magnetite.

Abbreviations: Alm = almandine component of Grt, cpxnite = clinopyroxenite, Cpx = clinopyroxene, Crd = corundum, Grs = grossular component in Grt, Grt = garnet, Ol = olivine, Pyr = pyrope component of Grt, Spl = spinel.

serpentinization of olivine in the sample as serpentine contains ~13% H₂O.

6. Analytical methods

Major and minor element concentrations were determined using a Philips PW 2400 X-ray fluorescent spectrometer (XRF) after fusing bulk rock powder with a flux composed of 78.5% Li₂B₄O₇ and 21.5% LiBO₂. Loss on ignition (LOI) was determined after placing 1 g of sample powder in an oven at 1050 °C for over 1.5 h. Trace elements, including rare earth elements (REE) of bulk rock were determined on a glass disk in the same way using a laser-assisted inductively-coupled plasma mass spectrometer (ICP-MS) described below as those in clinopyroxene grains. The concentrations of platinum group element (PGE) were determined by an isotopic dilution technique. Blanks were 0.002–0.007 ng Ir/g flux, 0.002–0.006 ng Os/g flux, 0.07–16 ng Pt/g flux, 0.03–0.9 ng Pd/g flux and 0.002–0.007 ng Ru/g flux. These values are negligible compared to the amounts in the samples, and thus blank corrections were not applied to the results.

Mineral compositions were determined using a CAMEBAX MBX electron probe in the wavelength dispersive mode. Counting times were 15–20 s per element, except for Ni (40 s). A 15 kV accelerating voltage and a 20 nA beam current were applied. The calibration used orthoclase (Si), wollastonite (Ca), synthetic spinel (Al), synthetic Cr₂O₃ (Cr), forsterite (Mg), synthetic MnTiO₃ (Mn and Ti), vanadium metal (V), albite (Na), fayalite (Fe in silicates), metallic Ni (Ni), and synthetic Fe₂O₂ (Fe in oxides). The Fe³⁺ contents of spinel were calculated assuming a stoichiometric composition.

Qualitative maps of Mg and Ca contents in garnet grains were obtained using a Philips Eagle III micro-X-ray fluorescent spectrometer. Counting times were 100 ms, a 15 kV accelerating voltage and a 400 μ A beam current were applied. Each analysed pixel represents a beam of 50- μ m diameter.

Two samples containing unaltered clinopyroxene grains were selected for *in-situ* trace-element analysis using a laser-assisted ICP-MS that consists of a Geolas 193 nm excimer laser system linked to a Finnigan-Matt Element XR high-resolution ICP-MS. The laser beam was guided through the objectives of a microscope, and focused on the sample surface to produce ablation pits of ~30–35 μ m diameter. Ablations were performed in a He gas atmosphere and the sample particles were introduced to the ICP-MS with He gas. The concentrations of these elements were calculated from the count ratios of isotopes of the elements to ⁴³Ca, and the concentrations of Ca and calibrated with the NIST 612 reference glass. One cycle of analysis started with the measurement of background values by blocking the laser beam from the sample, followed by the laser abrasion of samples. Each sample point was measured for at least three cycles while observing the ablation spectra. The precision and accuracy of the

analyses were checked with the glass disk made of USGS-BCR2 reference material USGS-BCR2G reference glass (Table 2).

7. Results

7.1. Mineral chemistry

7.1.1. Olivine

Olivine is free of mineral inclusions except for serpentine along fractures. Olivine contains relatively low Mg, with Mg# values (Mg/[Mg + Fe]) ranging from 0.74 to 0.83 (Table 3, Fig. 4). Olivine in dunite (RD59) has the highest Mg#, ~0.82–0.83 (Fig. 4), and that in olivine-rich wehrlite (RD57) also shows high values between 0.81 and 0.82. Olivine in other samples, wehrlite and clinopyroxenite, contains lower Mg#, <0.79 (Fig. 4). The composition of olivine in our samples is similar to those reported from garnet-bearing boulders in the area by previous workers (Abbott et al., 2005).

The values of Mg# are much lower than those of olivine in equilibrium with mantle peridotites (i.e., 0.90–0.92; Arai, 1994) and mantle xenoliths in kimberlites (Sato, 1977). Olivine in abyssal peridotite contain lower Mg and Ni compared to most mantle xenoliths (Sobolev et al., 2005; Seyler et al., 2007), but the observed Mg and Ni concentrations in olivine in the garnet peridotite are even lower than those in abyssal peridotite (Fig. 4).

7.1.2. Clinopyroxene

Clinopyroxene forms large, up to 5 mm, crystals, and is free of any mineral inclusions. It is diopsidic, ~Fs₄₅En₆Wo₄₉, with considerable Cr₂O₃, up to 0.45 wt.%, and the compositions are similar among different grains within one sample. Clinopyroxene contains high Mg# (0.86–0.90), low TiO₂, less than 0.35 wt.%, and plot in the field of subduction-related ultramafic cumulates (Fig. 5a) on the Al–Ti discrimination diagram of Loucks (1990). Clinopyroxene also has low Al₂O₃, less than 3 wt.% in most samples. Low Al compared to Si results in clinopyroxene plotting in the non-alkaline subduction-related cumulate field (Fig. 5b) on the Al–Si discrimination diagram of Le Bas (1962). The composition of clinopyroxene in garnet peridotite is distinctly different from Na- and Al-rich clinopyroxene in eclogites in other parts of the Rio San Juan Complex and in many other metamorphic terranes.

Clinopyroxene is partially to totally hydrated to form magnesiohornblende, tremolite, and chlorite.

7.1.3. Spinel

Spinel is present as inclusion in garnet, in the matrix, and in the kelyphitic aureoles of garnet (Figs. 3 and 6). Spinel is minor in volume, up to 4 vol.%. It is hercynite (Al-rich spinel) in wehrlite and clinopyroxenite. It has high Y_{Al} (Al/[Al + Cr]), greater than 0.96, and variable X_{Mg} (Mg/[Mg + Fe]), between 0.49 and 0.62. A similar

Table 2
Compositions of bulk rock samples and individual grains of clinopyroxene in RD40 and RD63.

	Det.l	Method	Bulk rock RD40	Bulk rock RD63	Bulk rock BCR2G	Std	BCR2 rec. value ^a	RD 40 grain 2	RD 40 grain 3	RD 40 grain 4	RD 63 grain 1	RD 63 grain 6	RD 63 grain 7	RD 63 grain 8	RD 63 grain 10	RD 63 grain 11	RD 63 grain 12	RD 63 grain 13
SiO ₂		xrf	41.93	42.14														
TiO ₂		xrf	0.105	0.124	2.57	0.27	2.26											
MgO		xrf	25.79	25.08														
Na ₂ O		xrf	0.16	0.16														
Fe ₂ O ₃ ^b		xrf	13.867	14.02														
Al ₂ O ₃		xrf	7.25	6.86														
CaO		xrf	8.45	8.64							24.4	24.4	24.6	24.5	24.3	24.4	24.4	24.4
K ₂ O	0.03	xrf	0.023	0.022				<0.077	<0.078	<0.072	0.134	<0.06	<0.06	0.149	0.409	0.640	0.161	<0.06
P ₂ O ₅		xrf	0.02	0.02														
MnO		xrf	0.203	0.201	0.20	0.009	0.18											
LOI ^c		xrf	1.9	2.95														
Ni ^d	7.2	xrf	344	317	13.0	1.54	13.0	216	162	190	115	95	124	172	106	162	99	99
Cr	1.4	xrf	266	292				2140	2370	1830	2120	763	1830	1510	1300	2300	1330	1270
Co		xrf	112	105														
V		xrf	86	103														
Sc		ICP	36.3	39.7														
Ba ^d	0.04	ICP	30.8	30.4	643	24.4	683	<0.11	0.26	0.276	5.82	<0.13	0.162	1.87	14.2	15.2	2.01	1.65
Rb ^d		ICP	0.59	1.11	47.7	1.60	48.0											
Sr ^d	0.015	ICP	50.6	45.4	318	5.31	346	13.1	13.7	13.1	19.4	12.8	12.1	20.2	19.0	25.6	13.9	12.8
Y ^d	0.014	ICP	1.76	2.14	29.8	0.92	37.0	5.28	6.09	5.7	3.63	6.43	4.34	5.72	4.7	6.32	4.35	4.27
Zr ^d	0.33	ICP	1.53	1.77	153	6.0	188	1.53	2.29	1.95	1.82	3.40	0.87	1.69	1.25	1.38	1.36	1.67
Nb ^d	0.008	ICP	0.031	0.029	11.4	0.3	13.1	0.02	<0.02	<0.02	0.01	<0.013	<0.02	<0.01	<0.01	<0.01	<0.02	
La ^d	0.003	ICP	0.176	0.143	23.3	0.65	25.0	0.220	0.203	0.196	0.146	0.185	0.099	0.184	0.169	0.140	0.170	0.184
Ce ^d	0.003	ICP	0.436	0.401	50.6	1.39	53.0	0.701	0.697	0.632	0.541	0.703	0.407	0.647	0.613	0.501	0.590	0.534
Pr ^d	0.002	ICP	0.070	0.074	6.19		6.8	0.149	0.138	0.134	0.124	0.160	0.098	0.158	0.129	0.114	0.129	0.096
Nd ^d	0.013	ICP	0.446	0.458	26.0	0.573	28.0	1.09	1.180	0.997	0.822	1.24	0.737	1.134	0.977	0.872	1.039	0.849
Sm ^d	0.025	ICP	0.158	0.215	5.93	0.210	6.70	0.510	0.610	0.544	0.386	0.671	0.461	0.596	0.497	0.476	0.419	0.357
Eu ^d	0.004	ICP	0.088	0.097	1.74	0.039	2.00	0.196	0.245	0.251	0.178	0.226	0.188	0.248	0.202	0.203	0.208	0.173
Gd ^d	0.024	ICP	0.255	0.317	5.77	0.188	6.80	0.725	0.884	0.844	0.611	1.005	0.722	0.889	0.759	0.657	0.622	0.689
Tb ^d	0.002	ICP	0.047	0.053	0.95	0.020	1.07	0.134	0.175	0.147	0.124	0.192	0.126	0.169	0.134	0.107	0.124	0.123
Dy ^d	0.011	ICP	0.354	0.392	5.70	0.208	6.38	1.02	1.21	1.11	0.828	1.29	0.939	1.20	1.01	0.856	0.914	0.905
Ho ^d	0.001	ICP	0.072	0.088	1.13	0.046	1.29	0.224	0.259	0.224	0.163	0.287	0.190	0.233	0.202	0.187	0.178	0.179
Er ^d	0.01	ICP	0.216	0.229	3.13	0.131	3.66	0.707	0.816	0.695	0.426	0.752	0.530	0.616	0.570	0.471	0.544	0.492
Tm ^d	0.007	ICP	0.027	0.031	0.45	0.020	0.54	0.085	0.102	0.091	0.045	0.108	0.081	0.097	0.082	0.068	0.072	0.068
Yb ^d	0.01	ICP	0.200	0.242	3.10	0.059	3.50	0.530	0.589	0.588	0.434	0.713	0.502	0.591	0.561	0.403	0.562	0.415
Lu ^d	0.00	ICP	0.032	0.035	0.44	0.008	0.51	0.085	0.088	0.089	0.060	0.092	0.065	0.067	0.070	0.060	0.060	0.056
Hf ^d	0.01	ICP	0.080	0.078	4.83	0.043	5.17	0.156	0.143	0.181	0.136	0.211	0.119	0.144	0.109	0.105	0.107	0.126
Ta ^d	0.005	ICP	0.008	0.005	0.72	0.019	0.78	<0.021	<0.011	0.011	<0.01	<0.008	<0.008	0.010	<0.008	<0.01	0.0095	<0.008
Pb ^d	0.007	ICP	2.47	2.54	10.7	0.408	11.0	0.057	0.076	0.067	0.368	0.035	0.040	0.538	1.530	0.794	0.430	0.155
Th ^d	0.001	ICP	0.013	0.012	5.31	0.111	6.20	0.101	0.077	0.149	0.008	0.014	0.028	0.020	0.021	0.019	0.007	0.024
U ^d	0.001	ICP	0.030	0.009	1.66	0.057	1.69	0.071	1.40	0.147	0.013	0.014	0.016	0.022	0.024	0.024	0.007	0.017

^a Recommended values of BCR2 from Wilson (1997).

^b Total Fe expressed as Fe₂O₃.

^c Loss on ignition (LOI) was determined after heating samples at 1050 °C for 1.5 hrs.

^d Concentrations were obtained using the laser-assisted ICP-MS from the count ratios of isotopes to ⁴³Ca. The isotopes used were ⁴⁹Ti, ⁵⁵Mn, ⁶¹Ni, ⁸⁵Rb, ⁸⁸Sr, ⁸⁹Y, ⁹⁰Zr, ⁹¹Zr, ⁹³Nb, ¹³⁷Ba, ¹³⁹La, ¹⁴⁶Ce, ¹⁴¹Pr, ¹⁴⁶Nd, ¹⁴⁷Sm, ¹⁵³Eu, ¹⁵⁷Gd, ¹⁵⁹Tb, ¹⁶³Dy, ¹⁶⁵Ho, ¹⁶⁷Er, ¹⁶⁹Tm, ¹⁷²Yb, ¹⁷⁵Lu, ¹⁷⁸Hf, ¹⁸¹Ta, ²⁰⁸Pb, ²³²Th, ²³⁸U. The detailed analytical procedure is described in Dorais and Tubrett (2008).

Table 3
Representative compositions of minerals.

	Olivine		Clinopyroxene			Garnet			Spinel	
	RD50 (8)	RD63 (2)	RD40 (12)	RD50 (4)	RD63 (12)	RD62-A	RD63	RD50-A	RD62-1	RD50
SiO ₂	38.8	38.1	52.6	53.0	52.2	39.98	39.42	38.64	0.05	0.05
TiO ₂	n.d.	n.d.	0.224	0.15	0.267	0.05	0	0.01	<0.01	<0.01
Al ₂ O ₃	n.d.	n.d.	2.55	2.15	2.73	22.57	23	21.91	63.13	62.48
Fe ₂ O ₃			0.934	0.81	0.76	1.47	0.56	1.81	3.00	3.01
Cr ₂ O ₃		n.d.	0.21	0.1	0.21	0.02	0.02	0	0.12	0.03
FeO	22.9	21.3	4.0	3.4	4.01	17.85	19.05	19.63	17.32	21.41
MnO	0.41	0.25	0.152	0.09	0.137	1.25	1.06	1.14	0.25	0.20
MgO	38.8	39.2	15.3	15.8	15.0	11.7	10.7	5.4	15.85	13.32
CaO	n.d.	n.d.	24.2	24.4	24.3	6.08	6.12	12.35	n.d.	n.d.
Na ₂ O	n.d.	n.d.	0.15	0.14	0.12	0.02	0.01	<0.02	n.d.	n.d.
ZnO	n.d.	n.d.	n.d.	n.d.	n.d.	n.d.	n.d.	n.d.	0.23	n.d.
NiO	0.06	0.07	n.d.	n.d.	n.d.	n.d.	n.d.	n.d.	n.d.	n.d.
Sum	100.9	98.9	100.2	100.1	99.77	100.99	99.95	100.89	100	100.7
X(Alm)						37.9	40.5	42.5		
X(Gros)						12.1	15.0	28.9		
X(Pyr)						43.6	40.6	20.8		
XFe ³⁺									0.03	0.03
YCr									0.12	0.03

composition with slightly higher X_{Mg} , 0.77, was reported by [Abbott et al. \(2005\)](#). Cr-rich spinel is observed as a relict in dunite and altered to Cr-rich magnetite.

Skeletal spinel with euhedral crystal outlines are locally preserved within garnet ([Fig. 3c, d](#)). This evidence suggests the destabilization of Al-spinel during the prograde metamorphism that formed garnet.

The composition of Al-rich spinel in wehrlite and clinopyroxenite contrasts with that in serpentinites in mélanges in the Rio San Juan Complex and along the major faults, which contain high Cr and similar Mg# ([Saumur et al., 2010](#)). The composition of hercynite in our sample is similar to those in metamorphosed ultramafic rocks reported by [Barnes and Roeder \(2001\)](#).

7.1.4. Garnet

Coarse-grained garnet contains many mineral inclusions, such as Al-spinel and corundum ([Figs. 3 and 6a, b](#)). The grains also contain late fractures that are filled by calcite ([Fig. 6b](#)). In addition, intensity maps of Mg K α ([Fig. 6a](#)) and Ca K α ([Fig. 6b](#)) of coarse-grained garnet show inclusions of earlier-formed small garnet. Individual inclusions of garnet contain Ca- and Al-rich cores and Mg-rich rims ([Fig. 6a, b](#)). The distribution and number of garnet inclusions are evident on the

Ca K α intensity map of garnet ([Fig. 6b](#)) as it shows Ca-rich cores of individual garnet inclusions. Rims of these small inclusions overlap with rims of other inclusions as if an aggregate of small inclusions of garnet is “cemented” by Ca-poor garnet ([Fig. 6b](#)).

The coarse grained garnet also contains late Mg-rich bands ([Fig. 6a](#)). The Mg-rich bands contain more Mg than the rims of small garnet inclusions and the main part of garnet. Because of the occurrence of these Mg-rich bands and numerous Ca- and Al-rich cores of small inclusions ([Fig. 6a, b](#)), the composition profile of a coarse-grained garnet shows irregular and sharp changes in the concentrations of Mg and Al ([Fig. 6c](#)). It is not clear why late Mg-rich garnet produced bands instead of an overgrowth ([Fig. 6c](#)).

In summary, three types of garnet are recognized within coarse-grained garnet; Ca- and Al-rich garnet in the cores of garnet inclusions, Ca- and Al-poor garnet in the rims of garnet inclusions and the main part of coarse garnet, and late Mg-rich bands. The compositional evolution of garnet suggests that the early garnet likely crystallized during the destabilization of Ca-Al phase(s). Higher contents of Mg in later garnet are consistent with the progressive increase in P - T ([Medaris, 1999](#)).

7.2. Corundum

Corundum occurs as irregularly-shaped inclusions (<50 μ m in size) in granoblastic garnet in close spatial association with green Al-spinel ([Fig. 3a, b, e](#)) and commonly near the boundary between Mg-poor and Mg-rich garnet. The texture suggests that corundum crystallized during garnet formation. Rare corundum occurs as an inclusion within Al-rich spinel outside garnet. The evidence suggests the change of Al-rich spinel to corundum and garnet.

Corundum is minor in volume, <1 vol.% of the rock, but the occurrence is ubiquitous among samples including clinopyroxenite and wehrlite and the occurrence is not related to grain size and texture of rocks. Corundum has a close to the ideal composition of Al₂O₃ with low concentrations of other elements, such as FeO (0.3–0.5 wt.%), CaO (<0.1 wt.%), MnO (<0.1 wt.%), and Cr₂O₃ (<0.1 wt.%).

7.2.1. Unidentified phase

An irregularly shaped unidentified phase is present together with corundum and spinel within garnet ([Fig. 3b](#)). It is transparent and optically isotropic probably due to a mixture of very fine-grained material. The compositions vary with high Ca, Si and Al. [Abbott et al.](#)

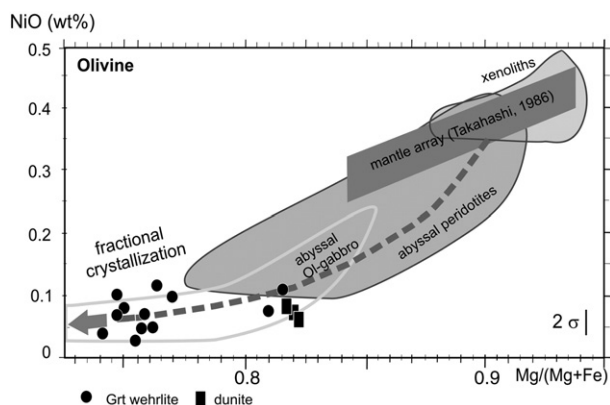


Fig. 4. NiO vs atomic ratio of Mg/(Mg + Fe) of olivine in garnet peridotites from the northern Dominican Republic. The data sources: the mantle array ([Takahashi, 1986](#)), abyssal peridotites ([Sobolev et al. 2005](#)), mantle xenoliths ([Sato, 1977](#)), and abyssal olivine (Ol) gabbro ([Suh et al., 2008](#)).

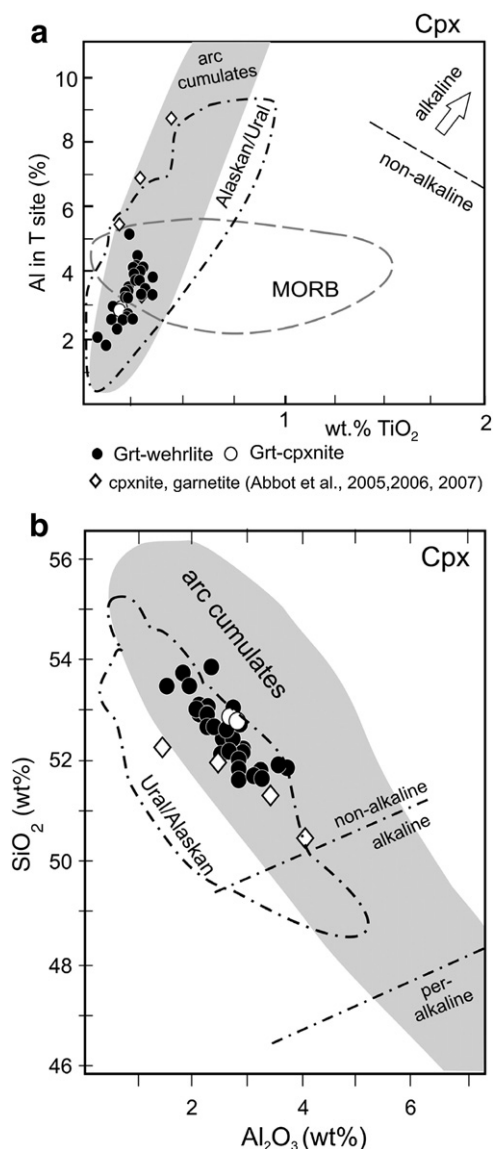


Fig. 5. Composition of clinopyroxene plotted on (a) the Al–Ti discrimination diagram of Loucks (1990) and (b) the Al–Si discrimination diagram of Le Bas (1962). The gray area for arc cumulates and the area shown with dashed line for mid-oceanic ridge basalts (MORB) are by Loucks (1990). Areas with dash-dot lines are Alaskan/Ural type ultramafic intrusions along subduction zones (Pettigrew and Hattori, 2006). Circles are garnet-bearing ultramafic rocks obtained this study. Open diamonds are clinopyroxene data of garnet-clinopyroxenites and garnetite in Abbott et al. (2005, 2006, 2007).

(2005) also noted the presence of an “unidentified phase” in corundum enclosed by garnet.

7.3. Bulk compositions

Samples contain low concentrations of compatible elements (<400 ppm Ni and <400 ppm Cr) except for olivine-rich RD57 and RD59 (Table 2). Even olivine-rich rocks contain significantly low values compared to the primitive mantle values (2625 ppm Cr and 1960 ppm Ni; McDonough and Sun, 1995). The data suggest that garnet peridotite is not a residue of mantle peridotite after partial melting. Instead, the garnet peridotite is a cumulate of melt. This interpretation is further supported by low concentrations of Ir-type PGE (Ir, Ru, and Os; Fig. 7, Table 4). Among PGE, Ir-type PGE is compatible with mantle minerals and remains in the residual mantle peridotites during partial melting (e.g., Righter et al., 2004; Brennan et al., 2005). A melt, therefore, contains low concentrations of Ir-type

PGE compared to the residual mantle peridotites and the cumulate from the melt also contains low concentration of Ir-type PGE.

The low concentrations of PGE in our garnet peridotite are in contrast to high PGE contents in serpentinites that occur as boulders along the Rio Cuevas and along the major faults (Fig. 7). High concentrations of Ir-type PGE in these serpentinites are consistent with their fore-arc mantle origin (Saumur et al., 2010).

Two samples, RD40 and RD63, were selected for detailed analysis of trace elements in the bulk and their clinopyroxene since clinopyroxene grains in these samples are relatively free of alteration (Supplemental diagram). Other minerals were not subjected to the trace element analysis because of their small size, irregular shape, and the presence of mineral inclusions and late fractures. For example, it was difficult to obtain reliable trace element data from coarse-grained garnet because it contains many inclusions and late fractures filled with calcite.

Trace elements of bulk rocks in these two were also analyzed by the identical method using the laser-assisted ICP-MS as the analysis of clinopyroxene so that there was no instrumental and analytical bias during the comparison of the two data sets due to different analytical techniques and possible incomplete digestion of bulk rock samples. The bulk rock chemical compositions show a subduction-related geochemical signature with high concentrations of fluid-mobile elements (Sr, U and Pb) and low concentrations of high field-strength elements (Nb, Th, Y and Zr) (Fig. 8a). Although these fluid-mobile elements are susceptible to alteration and metamorphism, similar element patterns in the two samples (Fig. 8) suggest that the observed geochemical signature of bulk rock likely reflects that of the original rocks. This is further supported by the trace element patterns of clinopyroxene grains described below.

The concentrations of Th are distinctly lower than those of U (Fig. 8) and Y also show minor depletion compared to elements with similar compatibilities. The values of Y/Y^* ($2 \times [Y]/[Ho] + [Er]$) where elements in square brackets are normalized values) are 0.83 and 0.89. The geochemical signature, low high-field strength elements relative to fluid-mobile elements, likely reflects that of the parental melt because these elements are not likely fractionated during the crystallization of olivine and clinopyroxene that do not incorporate much of these high-field strength elements. High-field strength elements have an affinity with oxides and they may be removed from the parental melt during oxide formation. There is no evidence suggesting this early crystallization of oxides in garnet peridotite. Cr-rich spinel is observed only in dunite, and the amount is minor as indicated by low Cr contents in bulk rock composition. Al-rich spinel appears to have crystallized late in most garnet peridotite. Both olivine and clinopyroxene are essentially free of mineral inclusions. Therefore, we suggest that high concentrations of fluid-mobile elements compared to high field-strength elements is the geochemical signature of the parental melt, and that the parental melt formed in the mantle wedge to acquire the subduction-related geochemical signature.

The bulk rock data also show minor positive anomalies of Eu (Fig. 8). The values of Eu/Eu^* for these samples are 1.18 for RD 40 and 1.32 for RD 63 (Fig. 8a). Plagioclase preferentially incorporates Eu as Eu^{2+} . Observed positive anomalies in the bulk rock, therefore, suggest that plagioclase likely crystallized as a cumulate phase. High CaO (~8.5 wt.%) and Al_2O_3 (~7 wt.%) in bulk rocks also support the presence of plagioclase in the original rocks.

7.4. Trace elements in clinopyroxene

The patterns of trace elements are similar among different clinopyroxene grains and, like the bulk rock, show low concentrations of high-field strength elements (Nb, Ta, Zr, Hf and Y), with high concentrations of fluid-mobile elements (U, Pb and Sr) (Fig. 8b). The data confirm that the high contents of fluid-mobile elements in bulk

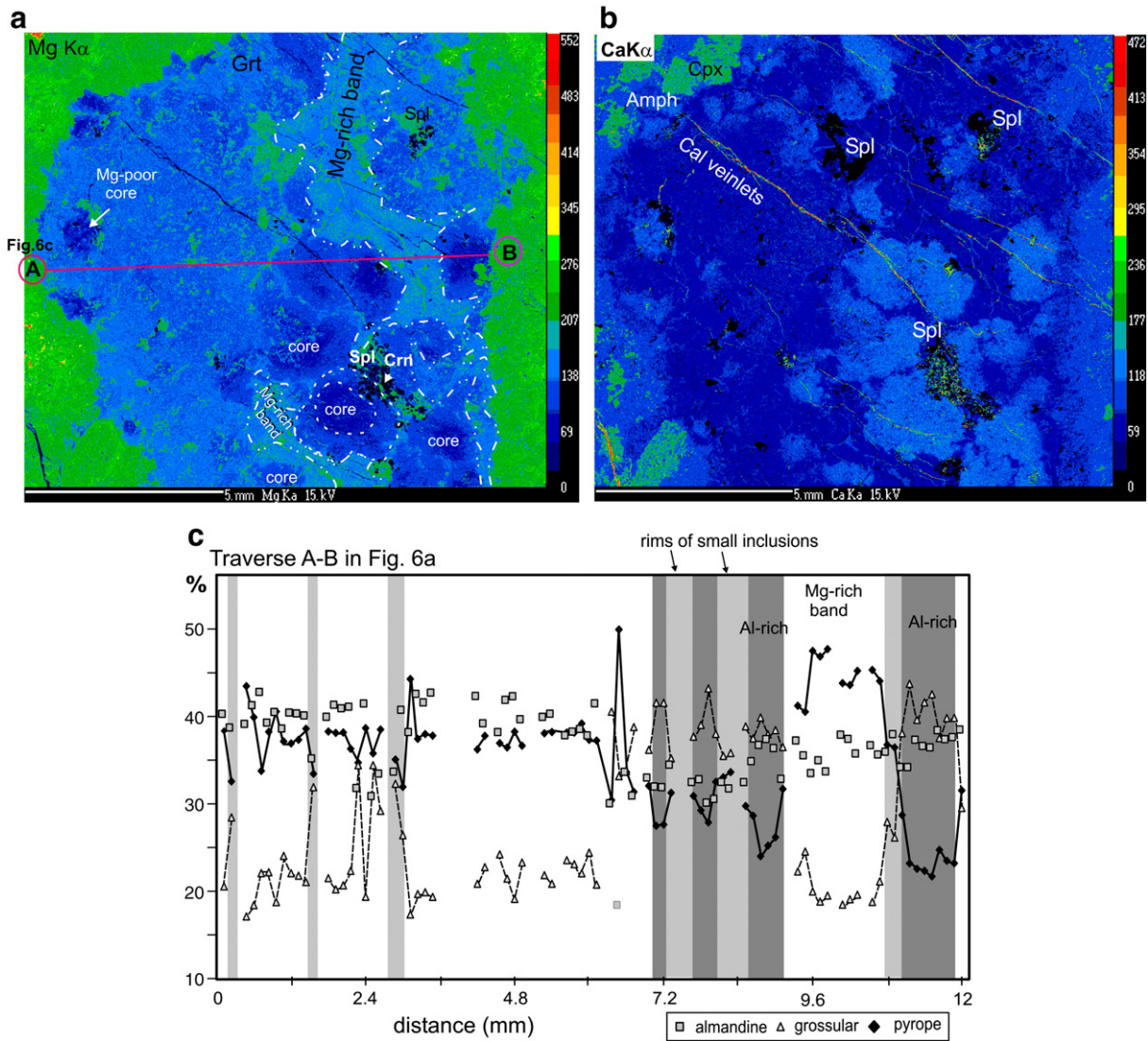


Fig. 6. Mg K α (a) and Ca K α (b) images of garnet (Grt) showing inclusions of small garnet, Al-spinel (Spl), corundum (Crn), and late high Mg bands (shown with white dash-dot lines in a). At least 16 inclusions of garnet are apparent in the garnet (b) and individual inclusions show Ca- and Al-rich cores and Mg-rich rims. The rim and core of one small grain are shown with dashed lines in panel a. A thick pink line between A and B corresponds to the compositional profile shown in panel c. The composition was determined at every 0.12 mm along the 12 mm length. Missing points are mineral inclusions. The traverse shows large compositional variations of Mg, Al and Ca because the traverse runs over several garnet inclusions and one Mg-rich band. Aluminum-rich and Ca-rich cores are shown in dark grey, and rims of inclusions in light grey in panel c. The Ca K α image also shows calcite (Cal) filling very late fractures.

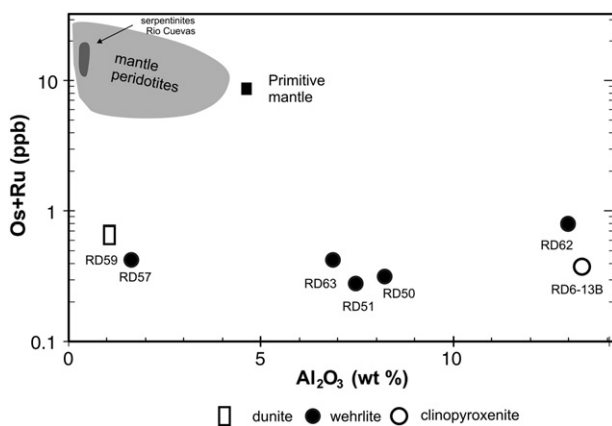


Fig. 7. Osmium plus Ru vs Al₂O₃ contents of bulk rock of garnet peridotites. The primitive mantle values are from McDonough and Sun (1995). For comparison, the values of serpentinite in the southern part of the Rio San Juan Complex (Saumur et al., 2010) are shown in dark grey area. The data sources of mantle peridotites are Gueddrat et al. (1996) and Wang et al. (2008). The values are tabulated in Table 4.

rock (Fig. 8a) are not due to alteration processes. Instead, the trace-element pattern of bulk rock reflects the geochemical character of the parental melt.

Table 4
Concentrations of platinum group elements (in ppb) and Al₂O₃ (in wt.%).

	Al ₂ O ₃	Os	Ir	Ru	Pt	Pd
RD 50	8.2	0.21	0.27	0.11	5.07	3.58
RD 51	7.46	0.077	0.19	0.21	5.03	4.13
RD 57	1.63	0.12	0.49	0.31	8.47	2.51
RD 59	1.06	0.20	0.95	0.47	8.3	7.07
RD 62	13.4	0.092	0.16	0.29	5.17	8.04
RD 63	6.86	0.19	0.17	0.25	49.1	29.3
RD 6-13B	13.0	0.55	0.19	0.25	1.86	7.48

The concentrations of PGE were determined by an isotopic dilution technique using a mixed spike solution enriched in ¹⁰¹Ru, ¹⁰⁵Pd, ¹⁹⁰Os, ¹⁹¹Ir and ¹⁹⁴Pt. The analytical procedure is essentially the same as that described by Hattori and Guillot (2007). PGEs were pre-concentrated in a Ni-sulphide bead that was dissolved in 6 N HCl, and the filtrate was dissolved in concentrated HNO₃ before analysis with a HP 4500 ICP-MS. The peak ratios of ⁹⁹Ru/¹⁰¹Ru, ⁹⁹Ru/¹⁰⁰Ru, ¹⁰⁵Pd/¹⁰⁶Pd, ¹⁰⁵Pd/¹⁰⁸Pd, ¹⁸⁹Os/¹⁹⁰Os, ¹⁹¹Ir/¹⁹³Ir, ¹⁹⁴Pt/¹⁹⁵Pd and ¹⁹⁴Pt/¹⁹⁶Pt were obtained with a HP-4500 ICP-MS.

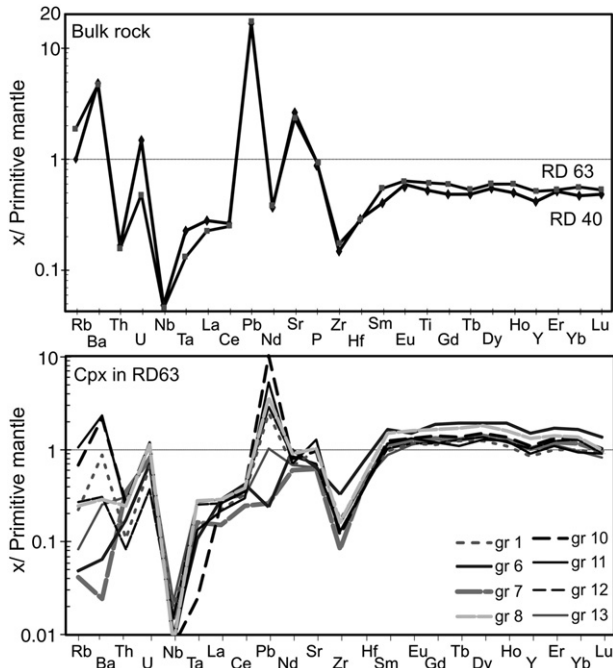


Fig. 8. Primitive mantle-normalized bulk rock and individual clinopyroxene composition. The numerical values are listed in Table 2. Primitive mantle values are from McDonough and Sun (1995).

Rare earth elements normalized to primitive mantle values show a slightly positive sloped pattern with low light REE, 0.1 to 1 times of primitive mantle values, and flat middle and heavy REE around the primitive mantle values (Fig. 9a, c). The pattern is distinctly different from REE patterns observed in clinopyroxene in garnet peridotite xenoliths (e.g., Simon et al., 2003; Ionov et al., 2005). In such rocks, clinopyroxene has a negatively sloped normalized pattern of REE with very low concentrations of heavy REE because heavy REE are incorporated into garnet.

8. Discussion

8.1. Primary mineralogy

Plagioclase is absent in the current garnet peridotite. However, the positive Eu anomalies of bulk rock suggest that plagioclase was present initially in the original rocks, but was changed to form new Al and Ca phases. Aluminum phases observed in the rocks are corundum, Al-rich spinel and garnet. Among the three, garnet is clearly a late phase based on abundant mineral inclusions and compositional zoning. Elevated Mg contents in rims of small garnet inclusions and late Mg-rich garnet bands (Fig. 6a) suggest that garnet crystallized during the prograde stage of *P-T* increase as Mg is preferentially incorporated in the garnet at higher *P* and higher *T* conditions (Medaris, 1999). This proposed interpretation is further supported by the trace-element patterns of clinopyroxene and bulk rocks (Fig. 9). Garnet preferentially incorporates heavy REE (e.g., Green et al., 2000; Hellebrand et al., 2002). If garnet was a magmatic phase, it would

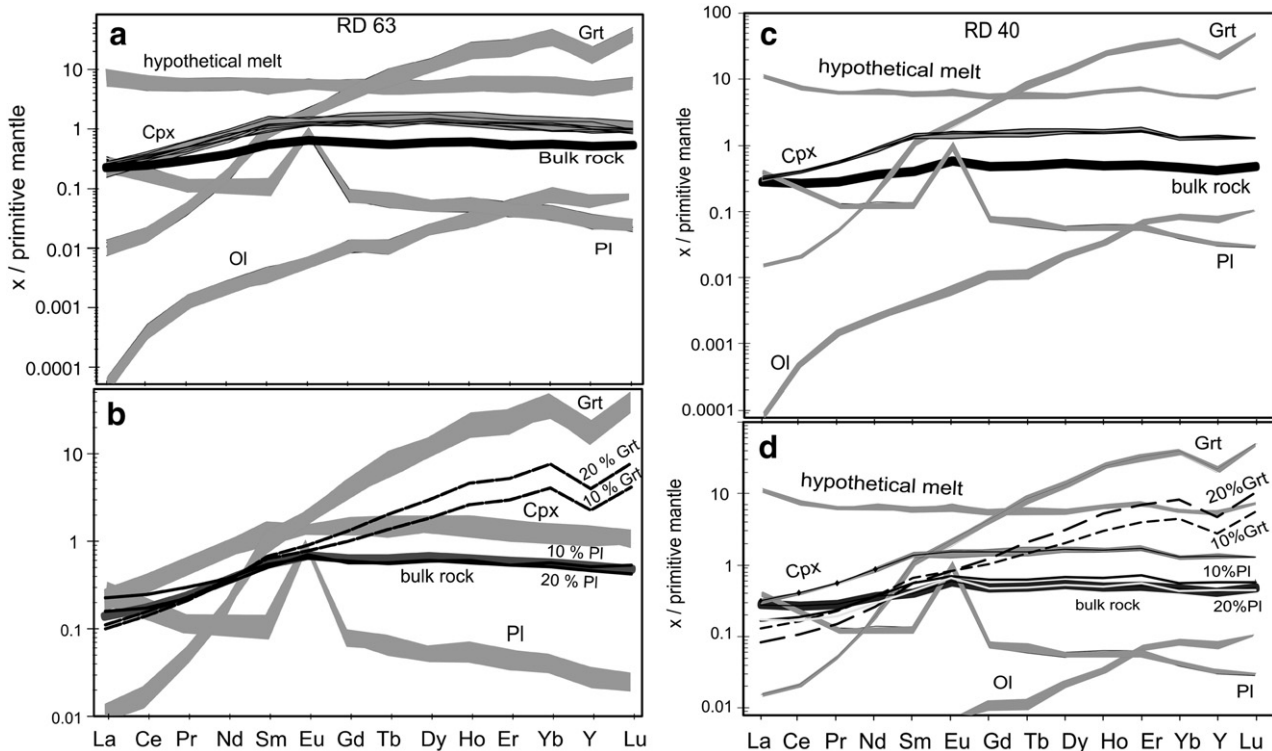


Fig. 9. Primitive-mantle normalized REE and Y for clinopyroxene grains, bulk rock, hypothetical melt, garnet, olivine and plagioclase for sample RD 63 (a) and sample RD 40 (c), and cumulates containing garnet or plagioclase (b and d). Note small positive anomalies of Eu ($Eu/Eu^* = 1.1$ and 1.3). The values of hypothetical melt, garnet, plagioclase and olivine are calculated from those of clinopyroxene. Bulk compositions of cumulates are calculated for four cases; (1) cumulates containing 20% garnet + 40% clinopyroxene + 40% olivine (dashed solid line depicted with 20% Grt), (2) 10% garnet + 45% clinopyroxene + 45% olivine (10% Grt), (3) 20% plagioclase + 40% clinopyroxene + 40% olivine (solid line depicted with 20% Pl), and (4) 10% plagioclase + 40% clinopyroxene + 40% olivine (10% Pl). Partition coefficients, *D*, between clinopyroxene and garnet and between clinopyroxene and melt used those in hydrous melt (10 wt.% H₂O) at 1200 °C by Green et al. (2000). *D* values between clinopyroxene and garnet are La = 20.8, Ce = 19.0, Pr = 10.7, Nd = 4.57, Sm = 1.26, Eu = 0.697, Gd = 0.357, Tb = 0.187, Dy = 0.125, Ho = 0.067, Er = 0.053, Yb = 0.034, Y = 0.062, Lu = 0.026. *D* values between clinopyroxene and melt are La = 0.0288, Ce = 0.055, Pr = 0.088, Nd = 0.135, Sm = 0.232, Eu = 0.229, Gd = 0.266, Tb = 0.274, Dy = 0.298, Ho = 0.247, Er = 0.236, Yb = 0.219, Y = 0.244, Lu = 0.178. The *D* values between olivine and melt and between plagioclase and melt used those listed in Hellebrand et al. (2002) and Norman et al. (2005), respectively.

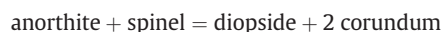
contain high concentrations of the heavy REE and so the bulk rock should also contain high concentrations of heavy REE. To evaluate the amount of possible magmatic garnet that might have crystallized in equilibrium with clinopyroxene, we calculated the REE contents of a hypothetical cumulate containing garnet, clinopyroxene and olivine. The REE contents of the hypothetical magmatic garnet and olivine are calculated using the *D* values between clinopyroxene and garnet by Hellebrand et al. (2002) and the *D* values for olivine given by Suhr et al. (1998) (Fig. 9b, d). Olivine can accommodate only very low concentrations of REE (e.g., Suhr et al., 1998). Therefore, the abundance of olivine in a cumulate has little effect on the abundance and REE in the rock. The results show that a cumulate containing even 10 wt.% magmatic garnet would have a distinct REE pattern with high concentrations of heavy REE in bulk rock (Fig. 9b, d). These high concentrations of heavy REE are not observed in our bulk rock samples, indicating that garnet was not a magmatic crystallization phase.

Next, the composition of a cumulate containing plagioclase was calculated, using the observed REE concentrations of clinopyroxene, and *D* values between clinopyroxene and anorthite (Norman et al., 2005). Plagioclase preferentially incorporates Eu^{2+} , producing positive Eu anomalies in REE patterns. The anomalies are greater in rocks that crystallized larger amount of plagioclase. The results show the observed REE patterns of bulk rocks are satisfactorily explained by a cumulate containing ~20 wt.% plagioclase together with olivine and clinopyroxene (Fig. 9b, d).

Abbott et al. (2005, 2007) postulated that partial melting occurred in the garnet peridotite after the solidification of the rock and that the partial melt is lost from the garnet peridotite. This suggests that the observed garnet peridotite is a residue of partial melting. However, if there had been a loss of melt, the residual rocks would have lost the incompatible elements that would have been preferentially incorporated into a melt, while compatible elements would have been retained in the residual rock. Among the REE, the light REE would have been lost to the melt and the heavy REE would have remain in the rock. The observed bulk rock compositions (thick dark lines in Fig. 9a and c) show no enrichment of heavy REE, suggesting that there is no evidence for a loss of partial melt from the rocks. Our interpretation is further supported by similar trace element patterns between bulk rock and clinopyroxene (Fig. 8) because incompatible elements (the elements in the left side of Fig. 8) would have been preferentially lost by a melt.

Abbott et al. (2005, 2006, 2007) also postulated corundum as a late magmatic phase formed from an evolved melt under high *P–T*. We discount this possibility because our data suggest that the solidification of the peridotite took place in the plagioclase peridotite field at shallow depths (Fig. 10) where corundum is not stable. Furthermore, the occurrence of corundum is ubiquitous in garnet grains in peridotite samples, and it is not restricted to late pegmatite phases. Therefore, we suggest that corundum is a metamorphic product of plagioclase breakdown, which occurs as aggregates in spatial association with Al-spinel within garnet.

Morishita and Arai (2001) suggested that corundum forms from plagioclase by the following metamorphic reaction:



In our samples, diopside is not spatially associated with corundum and no diopside is observed within garnet. Instead, corundum occurs between Ca-rich garnet and Mg-rich garnet within coarse grained garnet. Therefore, corundum in our samples likely formed by a different reaction path. To evaluate the crystallization conditions of corundum, we calculated the stability fields of metamorphic minerals in a rock having the bulk composition of representative garnet peridotite, sample, RD51, using the software Theriak-Domino (de Capitani and Brown, 1987; de Capitani, 1994) and the thermodynamic data of Berman (1988) at *P* between 0 and 30 kbar and *T* between 200 and 1200 °C

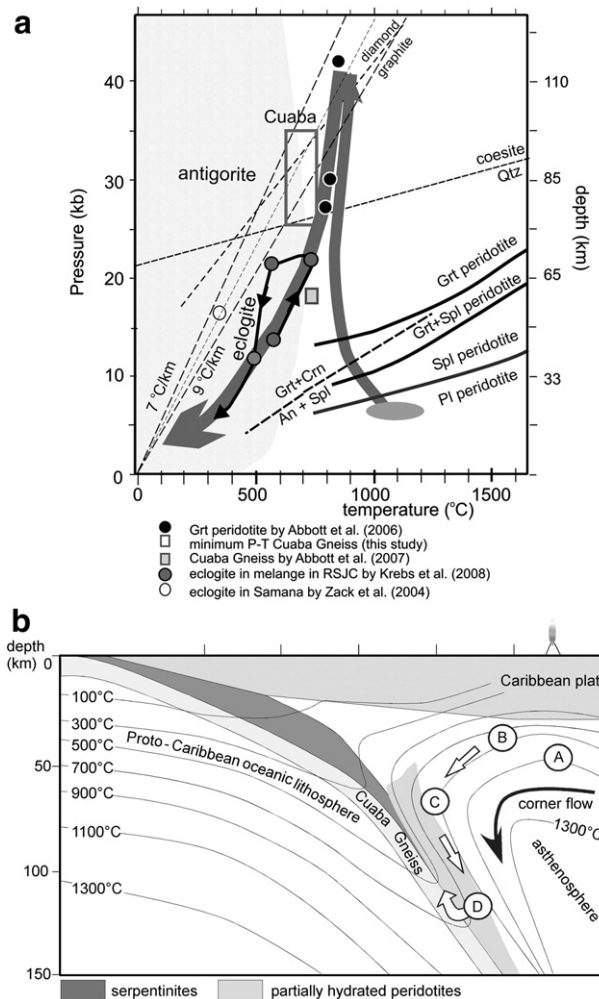


Fig. 10. (a) Schematic path of the garnet peridotite (thick gray curve with arrows) on *P–T* diagram. The *P–T* estimates of Grt peridotite and clinopyroxenite by Abbott et al. (2006) using Grt–Cpx–Ol–Spl thermobarometry (solid circles), and the estimates of eclogite associated with a serpentinite melange in the Rio San Juan Complex by Krebs et al. (2008) (grey circles), and the minimum *P–T* of eclogite in Cuaba Gneiss (large rectangular, this study), the estimate of Cuaba Gneiss by Abbott et al. (2007) is shown with an open rectangular. The peak *P–T* of lawsonite eclogite in the Samana peninsula in the same subduction zone calculated by Zack et al. (2004) is shown as an open circle. The stability fields of plagioclase-, spinel- and garnet peridotites were calculated using the bulk rock composition of sample RD51 (41.3 wt.% SiO_2 , 7.8 wt.% Al_2O_3 , 25.1 wt.% MgO , 13.9 wt.% Fe_2O_3 , 8.31 wt.% CaO , 0.8 wt.% Na_2O , 0.22 wt.% MnO) using the software Theriak-Domino (de Capitani and Brown, 1987; de Capitani, 1994) and the thermodynamic data of Berman (1988). The *P–T* of the reaction, anorthite + spinel = corundum + garnet (dashed line), was calculated using the same computer program. The initial condition contains spinel ($X_{\text{Mg}} = 0.6$ and $Y_{\text{Al}} = 1.0$) and the product garnet contains 0.5 grossular and 0.3 pyrope components. Antigorite stability field is after Ulmer and Trommsdorff (1995). (b) A schematic section showing the transport of the ultramafic cumulate. The original location is shown at A in the plagioclase-peridotite field of the forearc mantle of the Caribbean arc, the position B corresponds *P–T* conditions where corundum starts crystallizing, the position C and D are *P–T* conditions estimated by Abbott et al. (2006) using Grt–Cpx–Spl–Crm thermobarometry, and Grt–Cpx–Ol–Spl thermobarometry, respectively. As the Proto-Caribbean oceanic crust formed at an ultraslow spreading ridge (Meschede and Frisch, 1998), the oceanic lithosphere contained abundant serpentinites and its subduction produced a serpentinite-rich accretionary prism and a serpentinite-rich subduction channel (Gorczyk et al., 2007). The temperature contours and the distribution of partially hydrated forearc mantle peridotite are after Gorczyk et al. (2007).

(Fig. 10a). The garnet peridotite that would formed in this system contains olivine with Mg# 0.80, clinopyroxene with Mg# 0.90 and garnet with 0.45 pyrope and 0.33 grossular components. These mineral compositions are in good agreement with the measured compositions of olivine, clinopyroxene, and the Mg-rich portions of garnet (Fig. 6c).

Our calculation, however, could not produce Ca-rich garnet at any T and P . Furthermore, corundum forms only at low T , below 450 °C. The results suggest that the two phases (corundum and Ca-rich garnet) cannot be crystallized in equilibrium with the bulk rocks. We suggest that the two phases formed in an environment with limited reactions with other phases. Considering the fact that corundum occurs in spatial association with Al-spinel in the core of Ca-rich garnet (Fig. 3a, b), we suggest that the two phases formed from plagioclase and spinel in a restricted environment dominated by local equilibrium:

anorthite + spinel = corundum + Ca-rich garnet

To confirm our proposed interpretation, we calculated the metamorphic mineral assemblage starting from a mixture of anorthite and Al-spinel ($X_{\text{Mg}} = 0.6$, $Y_{\text{Al}} = 1.0$). This spinel composition is similar to the measured composition of spinel inside Ca-garnet. An assemblage of corundum plus Ca-rich garnet crystallizes from anorthite and spinel at P between 7 and 11 kbar and T greater than 700 °C (Fig. 10a). The garnet produced in this reaction contains high grossular component, 0.5, and low pyrope component, 0.3. The composition of the garnet is similar to the observed of Ca-rich garnet observed in the cores of small garnet inclusions (Fig. 6c).

In summary, we suggest the following sequence of mineral crystallization. Olivine, clinopyroxene, plagioclase and spinel solidified from a mafic melt as cumulate phases at relatively low P , <5–7 kbar, in the plagioclase peridotite field (Fig. 10a). During the prograde metamorphism, plagioclase and spinel were locally destabilized to form Ca- and Al-rich garnet and corundum at P over 10 kbar (Fig. 10a). Once the plagioclase had been consumed, Ca-poor garnet started to crystallize at the expense of spinel and it surrounded earlier formed Ca- and Al-poor garnet grains. These small garnet grains are subsequently “cemented” by Mg-rich garnet to form coarse-grained garnet. Further prograde metamorphism produced high Mg-garnet as bands and patches within coarse-grained garnet.

8.2. Parental melt of garnet peridotite

The bulk-rock compositions and trace-element contents of clinopyroxene suggest that garnet peridotite is a cumulate of a melt formed in the mantle wedge. Our interpretation is consistent with the compositions of olivine and clinopyroxene, and low concentrations of Ir-type PGE. Olivine shows overall low contents of Ni and Mg (Fig. 4), which are too low to be considered as residual mantle peridotite. Clinopyroxene contains low Al and Ti and plots in the arc cumulate field (Fig. 5a, b).

Low Mg and Ni contents in olivine suggest that the parental melt for the crystallization of olivine was evolved. The Mg# of this melt is evaluated using the composition of Ol based on the Fe–Mg exchange coefficient, K_d , between Ol and melt. The K_d value varies with T , P and the composition of melt (Toplis, 2005), but the P effect on K_d is small, 0.01 per kbar. The composition of melt and T cancel each other on their effect on K_d ; higher T increases K_d and lower Si decreases K_d . Therefore, we use 0.3 for K_d , a commonly observed value in natural rocks and in experimental systems (Roeder and Emslie, 1970; Falloon and Danyushevsky, 2000). The calculated Mg# of the melt is 0.44–0.58.

There are two possible sites for the production of subduction-related melt; the forearc mantle or subarc mantle. We suggest that the parental melt for the garnet peridotites likely formed in the subarc mantle since magmatism in the forearc mantle is characterized by a high Mg melt, which produces boninites. Boninitic melt contains low concentrations of incompatible elements compared to arc magmas as the source mantle is highly refractory, yet Si contents are high (e.g., Stern and Bloomer, 1992). Most boninites contain high Mg#, >0.80, and low REE, similar to primitive mantle values (e.g., Stern and Bloomer, 1992; Tribuzio et al., 2008). Olivine in boninites is

characterized by high Mg#, commonly over 0.90 (e.g., Walker and Cameron, 1983; Bloomer and Hawkins, 1987), reflecting the high Mg# of the melt. Cr-spinel is a common accessory phase in boninites and has high Cr, Cr/(Cr + Al) over 0.8 (Walker and Cameron, 1983; Barnes and Roeder, 2001). Furthermore, high H₂O contents in boninitic magma suppress the crystallization of plagioclase, implying that plagioclase is rare except for evolved boninite magmas and high Ca-type boninites (e.g., Falloon and Crawford, 1991). Instead, enstatitic orthopyroxene is common in boninites including Ca-type boninites and their cumulates (e.g., Tribuzio et al., 2008). These characteristics of boninites and boninitic cumulates differ significantly from the observed mineralogy, mineral chemistry and bulk compositions of our peridotite in northern Dominican Republic. The composition of the hypothetical melt of our samples contains ~5 times the primitive mantle values of REE with very minor enrichment in light REE, reaching ~10 times that of primitive mantle values (Figs. 9a, c). Therefore, we conclude that the melt for our ultramafic cumulates was not likely generated in the forearc mantle, but rather in the subarc mantle below the Caribbean arc.

8.3. Transport of peridotite

The assemblage of garnet + clinopyroxene + spinel + olivine yielded 27–30 kbar and 807–838 °C in garnet peridotite and garnet clinopyroxenite and 42 kbar and 867 °C in one garnet peridotite (Abbott et al., 2006) (Fig. 10a). These estimated P – T conditions are comparable to that for Cuaba Gneiss. Abbott et al. (2007) estimated the minimum conditions of 18 kbar and 730 °C for the metamorphism of the Cuaba Gneiss. We also calculated the peak metamorphic condition of the Cuaba Gneiss using the bulk composition of eclogite samples and the maximum pyrope component (23%) of the cores of garnet. The compositions of cores were used for the calculation because rims of garnet subjected to partial hydration. The calculation using the Theriak-Domino software (de Capitani and Brown, 1987; de Capitani, 1994) and the thermodynamic data of Berman (1988) yielded the metamorphic P ranging between 25 and 35 kbar and T between 650 and 750 °C (Fig. 10a). These P – T values corresponds to those of a subduction channel at depths up to ~120 km (Fig. 10a), yielding a geothermal gradient of 7.3 °C/km for the subduction channel. This value is similar to that of ~8 °C/km estimated for the same subduction zone based on the P – T conditions, 360 °C and 16 kbar, of a lawsonite eclogite in Samana Peninsula, eastern tip of the Hispaniola (Zack et al., 2004). These values are similar to those commonly observed in subduction zones (e.g., Agard et al., 2008; Guillot et al., 2009). The data suggest that the peridotite was present in a cool subduction channel with a low geotherm (Fig. 10a).

Two questions arise: how the garnet peridotite reached the subduction channel and what is its relationship with the Cuaba Gneiss. To reach the depth and T in the subduction channel, the ultramafic cumulate had to be dislodged from the subarc lithospheric mantle, and transported from the subarc mantle towards the subduction plate, which has a horizontal distance of more than 100 km in most subduction zones (e.g., Syracuse and Abers, 2006, Fig. 10b). Such processes require an active mantle flow (Fig. 10b). Rare occurrences of garnet peridotites suggest that such strong mantle flow may not be common in oceanic subduction zones.

Mantle corner flow in the wedge mantle required a strongly coupled interface between the subducting and overlying plates and a rheologically weak mantle wedge (Arcay et al., 2007). Therefore, the flow is faster where the interface between the subducting and overlying plates is poorly lubricated. It has been known that lubricants in subduction zone include trench-fill sediments, the fluids expelled from these sediments at shallow levels, and serpentinites at deeper levels (e.g., Guillot et al., 2001, 2009; Lamb, 2006). Such lubrication develops with time hence is not available during the initial stage of subduction. At the very start of a subduction system, the overlying

plate and subducting plate are not even fully separated. This means that the mantle flow in the wedge is very strong in the very initial stage of subduction (e.g., Arcay et al. 2007). Therefore, we suggest that the horizontal transport of cumulate from the subarc to the subduction channel likely took place in the very early stage of the westward subduction of Proto-Caribbean oceanic lithosphere. Pindell et al. (2005) estimated that this initiation of the subduction took place at around ~120 Ma.

The proposed interpretation is supported by an anti-clockwise P – T path of an eclogite (Fig. 10) from the Rio San Juan Complex, documented by Krebs et al. (2008). An anti-clockwise path is not common in subduction zones, but expected during the initiation of subduction before a subduction zone has reached a thermal steady state condition (e.g., Krogh et al., 1994).

The model calculation by Arcay et al. (2007) shows that the subducting and overlying plates are being decoupled, that the mantle wedge becomes progressively hydrated, and that the overlying plate is thermal thinned during the first 10 to 20 Ma. This thermal thinning might have been responsible for the thermal erosion of the subarc mantle and its partial melting at shallow level to form the parental melt of the peridotite (Fig. 10b, step A). The strong coupling of two plates in the initial stage of the subduction likely caused a strong mantle corner flow to drag the subarc mantle peridotite to the interface between two plates (Fig. 10b, steps B and C). The P – T conditions of the metamorphism of the garnet peridotite suggests that it was subsequently pulled down in the subduction channel to a depth of 120 km (Fig. 10b, steps C and D).

The subducted Proto-Caribbean oceanic lithosphere formed at an ultraslow spreading ridge (Meschede and Frisch, 1998). Therefore, it contained abundant serpentinites (Krebs et al., 2008; Saumur et al., 2010). The subduction of such a serpentinite-rich oceanic lithosphere can quickly hydrate the overlying mantle wedge, which rheologically weakens the mantle wedge and contributes to an active mantle flow (e.g., Gorczyk et al., 2007). In addition, the subduction of serpentinite-rich oceanic crust produces a wide serpentinite-rich subduction channel, which is now exposed as serpentinite mélanges in the Rio San Juan Complex (Fig. 1b) (Krebs et al., 2008). A serpentinite-rich subduction channel produces enhanced channel flow (Gorczyk et al., 2007). The subducted garnet peridotite in the subduction channel was exhumed together with the Cuaba Gneiss in the well-developed return flows in the subduction channel. Within the subduction channel, rocks originated from the subducting oceanic plate mingle with rocks originated from the subarc mantle. This mechanism may explain the spatial association of UHP rocks of different origins along the Rio Cuevas; oceanic Cuaba Gneiss, subarc peridotite, and mantle wedge serpentinites. The proposed process also explains the lack of deformation fabrics in garnet peridotite because the strain was likely absorbed by the surrounding serpentinites.

9. Conclusions

Mineral chemistry of olivine and clinopyroxene and bulk rock compositions suggest that corundum-bearing garnet peridotites and clinopyroxenites are cumulates of a melt formed in the mantle wedge underlying the Cretaceous Caribbean arc. The melt solidified as plagioclase-bearing ultramafic rocks at shallow depth, ~35 km below the arc. The cumulate rocks were then dragged by a strong mantle flow towards the subduction plane, and incorporated into the subduction channel, which brought them down to a depth of ~120 km, along the subduction plate. Plagioclase in the original cumulates changed to spinel, corundum and garnet during prograde metamorphism. These events likely took place during the initiation of the westward subduction of the Proto-Caribbean oceanic lithosphere, when the lack of a lubricating layer along the interface between the subducting and overlying plates likely produced a strong mantle flow in the overlying mantle wedge. The viscous mantle flow was strong enough

to dislodge the cumulate from the subarc mantle, and dragged it to the subduction channel. The garnet peridotite was then exhumed together with the subducting oceanic gabbro (Cuaba Gneiss) within the well-developed serpentinite subduction channel.

Acknowledgements

We thank Peter Jones at Carleton University for his assistance with the electron microprobe analysis, Monika Wilk-Alemany, Mahmood Salman, and Nimal De Silva for analytical assistance, Ronald Hartree for XRF analyses, George Mrazek for preparation of polished sections at the University of Ottawa. Laser-assisted ICP-MS analysis was carried out at Inco Innovation Centre, X-ray maps at the Laboratoire Magmas et Volcans of Clermont-Ferrand. The project was funded in part by a Discovery Grant from the Natural Science and Engineering Research Council of Canada to KHH and grants under the DYETI program of INSU-CNRS to SG. We thank Ian Buick, Journal Editor, Hannes Brueckner and one anonymous referee for their helpful suggestions.

Appendix A. Supplementary data

Supplementary data associated with this article can be found, in the online version, at doi:10.1016/j.lithos.2009.10.010.

References

- Abbott Jr., R.N., Draper, G., Keshav, S., 2005. UHP magma paragenesis, garnet peridotite and garnet clinopyroxenite: an example from the Dominican Republic. *International Geology Review* 47, 233–247.
- Abbott Jr., R.N., Draper, G., Broman, B.N., 2006. P – T path for ultrahigh-pressure garnet ultramafic rocks of the Cuaba Gneiss, Rio San Juan Complex, Dominican Republic. *International Geology Review* 48, 778–790.
- Abbott Jr., R.N., Broman, B.N., Draper, G., 2007. UHP magma paragenesis revisited, olivine clinopyroxenite and garnet-bearing ultramafic rocks from the Cuaba Gneiss, Rio San Juan Complex, Dominican Republic. *International Geology Review* 49, 572–586.
- Arai, S., 1994. Compositional variation of olivine-chromian spinel in Mg-rich magmas as a guide to their residual spinel peridotites. *Journal of Volcanology and Geothermal Research* 59, 279–293.
- Arcay, D., Tric, E., Doin, M.P., 2007. Slab surface temperature in subduction zones: influence of the interplate decoupling depth and upper plate thinning processes. *Earth and Planetary Science Letters* 255, 324–338.
- Agard, P., Yamamoto, P., Jolivet, L., Burov, E., 2008. Discontinuous exhumation of oceanic crust: insights from blueschists and eclogites into the subduction channel. *Earth Science Reviews* 92, 53–79.
- Barnes, S.J., Roeder, P.L., 2001. The range of spinel compositions in terrestrial mafic and ultramafic rocks. *Journal of Petrology* 42, 2279–2302.
- Berman, R.G., 1988. Internally-consistent thermodynamic data for minerals in the system. *Journal of Petrology* 29, 445–522.
- Bloomer, S.H., Hawkins, J.W., 1987. Petrology and geochemistry of boninite series volcanic rocks from the Mariana trench. *Contributions to Mineralogy and Petrology* 97, 361–377.
- Brenan, J.M., McDonough, W.F., Ash, R., Brenan, J.M., McDonough, W.F., Ash, R., 2005. An experimental study of the solubility and partitioning of iridium, osmium and gold between olivine and silicate melt. *Earth and Planetary Science Letters* 237, 855–872.
- Brueckner, H.K., Medaris, L.G., 2000. A general model for the intrusion and evolution of 'mantle' garnet peridotites in high-pressure and ultra-high-pressure metamorphic terranes. *Journal of Metamorphic Geology* 18, 123–133.
- de Capitani, C., 1994. Gleichgewichts-Phasendiagramme: Theorie und Software. Beihefte zum *European Journal of Mineralogy* 72. Jahrestagung der Deutschen Mineralogischen Gesellschaft 6, 48.
- de Capitani, C., Brown, T.H., 1987. The computation of chemical equilibrium in complex systems containing non-ideal solutions. *Geochimica et Cosmochimica Acta* 51, 2639–2652.
- Dolan, J.F., Mullins, H.T., Wald, D.J., 1–61, 1998. Active tectonics of the north-central Caribbean; oblique collision, strain partitioning, and opposing subducted slabs. In: Dolan, J.F., Mann, P. (Eds.), *Active Strike-Slip and Collisional Tectonics of the Northern Caribbean: Geological Society of America Special Paper*, 326, pp. 1–61.
- Draper, G., Nagle, F., 1991. Geology, structure, and tectonic development of the Rio San Juan Complex, northern Dominican Republic. In: Mann, P., Draper, G., Lewis, J.F. (Eds.), *Geologic and tectonic development of the North America–Caribbean plate boundary in Hispaniola: Geological Society of America Special Paper*, 262, pp. 77–95.
- Dorais, M.J., Tubrett, M., 2008. Identification of a subduction zone component in the Higganum dike, Central Atlantic Magmatic Province: A LA-ICPMS study of clinopyroxene with implications for flood basalt petrogenesis. *Geochemistry, Geophysics, Geosystems* 9, Q10005. doi:10.1029/2008GC002079.

- Enami, M., Mizukami, T., Yokoyama, K., 2004. Metamorphic evolution of garnet-bearing ultramafic rocks from the Gongen area, Sanbagawa belt, Japan. *Journal of Metamorphic Geology* 22, 1–15.
- Falloon, T.J., Crawford, A.J., 1991. The petrogenesis of high-calcium boninite lavas dredged from the northern Tonga ridge. *Earth and Planetary Science Letters* 10, 375–394.
- Falloon, T.J., Danyushevsky, L.V., 2000. Melting of refractory mantle at 1.5, 2 and 25 GPa under anhydrous and H₂O-undersaturated conditions: Implications for the petrogenesis of high-Ca boninites and the influence of subduction components of mantle melting. *Journal of Petrology* 41, 257–283.
- Girardeau, J., Ibaguchi, J.I.G., 1991. Pyroxenite-rich peridotites of the Cabo Ortegal complex (Northwestern Spain): evidence for large-scale upper mantle heterogeneity. In: Menzies, M.A., Dupuy, C., Nicolas, A. (Eds.), *Journal of Petrology Lherzolites Special Volume*, pp. 135–154.
- Goncalves, P., Guillot, S., Lardeaux, J.-M., Nicollet, C., de Lepinay, B.M., 2000. Thrusting and sinistral wrenching in a pre-Eocene HP–LT Caribbean accretionary wedge (Samaná Peninsula, Dominican Republic). *Geodinamica Acta* 13, 119–13221.
- Gorczyk, W., Guillot, S., Gerya, T.V., Hattori, K.H., 2007. Asthenospheric upwelling, oceanic slab retreat and exhumation of UHP mantle rocks: insights from Greater Antilles. *Geophysical Research Letters* 34, L21309. doi:10.1029/2007GL031059.
- Green, T.H., Blundy, J.D., Adam, J., Yaxley, G.M., 2000. SIMS determination of trace element partition coefficients between garnet, clinopyroxene, and hydrous basaltic liquids at 2–7.5 GPa and 1080–1200 °C. *Lithos* 53, 165–187.
- Gueddari, K., Piboule, M., Amossé, J., 1996. Differentiation of platinum group elements (PGE) and of gold during partial melting of peridotites in the lherzolitite massifs of the Betico–Rifean range (Ronda and Beni Bousera). *Chemical Geology* 134, 181–197.
- Guillot, G., Hattori, K., de Sigoyer, J., Nägler, T., Auzende, A.L., 2001. Evidence of hydration of the mantle wedge and its role in the exhumation of eclogites. *Earth and Planetary Science Letters* 193, 115–127.
- Guillot, S., Hattori, K.H., Agard, P., Schwartz, S., Vidal, O., 2009. Exhumation processes in oceanic and continental contexts: a review. In: Lallemand, S., Funicello, F. (Eds.), *Subduction Zone Geodynamics*. Springer-Verlag, pp. 175–205. doi:10.1007/978-3-540-87974-9.
- Hattori, K.H., Guillot, S., 2007. Geochemical character of serpentinites associated with high- to ultrahigh-pressure metamorphic rocks in the Alps, Cuba, and the Himalayas: recycling of elements in subduction zones. *Geochemistry Geophysics Geosystems* 8, Q09010. doi:10.1029/2007GC001594.
- Hattori, K., Wallis, S., Enami, M., Mizukami, T., 2009. Subduction of mantle wedge peridotites: evidence from the Higashi-akaishi ultramafic body in the Sanbagawa metamorphic belt. *Island Arc*. doi:10.1111/j.1440-1738.2009.00696.x.
- Hellebrand, E., Snow, J.E., Hoppe, P., Hofmann, A.W., 2002. Garnet-field melting and late-stage refertilization in “residual” abyssal peridotites from the central Indian Ridge. *Journal of Petrology* 43, 2305–2338.
- Ionov, D.A., Blichert-Toft, J., Weis, D., 2005. Hf isotope compositions and HREE variations in off-craton garnet and spinel peridotite xenoliths from central Asia. *Geochimica et Cosmochimica Acta* 69, 2399–2418.
- Kornprobst, J., Piboule, M., Roden, M., Tabit, A., 1990. Corundum-bearing garnet clinopyroxenites at Beni Bousera (Morocco): original plagioclase-rich gabbros recrystallized at depth within the mantle? *Journal of Petrology* 31, 717–745.
- Krebs, M., Maresch, W.V., Schertl, H.P., Münker, C., Baumann, A., Draper, G., Idlemann, B., Trapp, E., 2008. The dynamics of intra-oceanic subduction zones: a direct comparison between fossil petrological evidence (Rio San Juan Complex, Dominican Republic). *Lithos* 103, 106–137.
- Krogh, E., Oh, C.W., Liou, G., 1994. Polyphase and anticlockwise *P–T* evolution for Franciscan eclogites and blueschists from Jenner, California, USA. *Journal of Metamorphic Geology* 12, 121–134.
- Lamb, S., 2006. Shear stresses on megathrusts: implications for mountain building behind subduction zones. *Journal of Geophysical Research* 111, B07401. doi:10.1029/2005JB003916.
- Le Bas, M.J., 1962. The role of aluminum in igneous clinopyroxenes with relation to their parentage. *American Journal of Science* 260, 267–288.
- Lewis, J.F., Draper, G., Bourdon, C., Bowin, C., Mattson, P.O., Maurrasse, F., Nagle, F., Pardo, G., 1990. Geology and tectonic evolution of the northern Caribbean margin. In: Dengo, G., Case, J.E. (Eds.), *The Caribbean Region: Geological Society of America, The Geology of North America*, H, pp. 77–140.
- Loucks, R.R., 1990. Discrimination of ophiolitic from nonophiolitic ultramafic–mafic allochthons in orogenic belt by the Al/Ti ratio in clinopyroxene. *Geology* 18, 346–349.
- Medaris, L.G., 1999. Garnet peridotites in Eurasian high-pressure and ultrahigh-pressure terranes: a diversity of origins and thermal histories. *International Geology Review* 41, 799–815.
- Meschede, M., Frisch, W., 1998. A plate-tectonic model for the Mesozoic and early Cenozoic history of the Caribbean Plate. *Tectonophysics* 296, 269–291.
- McDonough, W., Sun, S.S., 1995. The composition of the earth. *Chemical Geology* 120, 223–253.
- Morishita, T., Arai, S., 2001. Petrogenesis of corundum-bearing mafic rock in the Horoman peridotite complex, Japan. *Journal of Petrology* 42, 1279–1299.
- Morishita, T., Arai, S., Gervilla, F., 2001. High-pressure aluminous mafic rocks from the Ronda peridotite massif, southern Spain: significance of sapphirine- and corundum-bearing mineral assemblages. *Lithos* 57, 143–161.
- Morishita, T., Arai, S., Ishida, Y., 2007. Occurrence and chemical composition of amphiboles and related minerals in corundum-bearing mafic rock from the Horoman Peridotite Complex, Japan. *Lithos* 95, 425–440.
- Norman, M., Garcia, M.O., Pietruszka, A.J., 2005. Trace-element distribution coefficients for pyroxenes, plagioclase, and olivine in evolved tholeiites from the 1955 eruption of Kilauea Volcano, Hawai‘i, and petrogenesis of differentiated rift-zone lavas. *American Mineralogist* 90, 888–899.
- Pettigrew, N.T., Hattori, K.H., 2006. The Quetico Intrusions of Western Superior Province: Neo-Archean examples of Alaskan/Ural-type mafic–ultramafic intrusions. *Precambrian Research* 149, 21–42.
- Pindell, J.L., Kennan, L., Maresch, W.V., Stanek, K.P., Draper, G., Higgs, R., 2005. Plate-tectonics and crustal dynamics of circum-Caribbean arc–continent interactions: tectonic controls on basin development in Proto-Caribbean margins. In: Avé Lallemand, H.G., Sisson, V.B. (Eds.), *Caribbean–South American plate interactions, Venezuela: Geological Society of America Special Paper*, 394, pp. 7–52.
- Prentice, C.S., Mann, P., Pena, L.R., Burr, G., 2003. Slip rate and earthquake recurrence along the central Septentrional fault, North American–Caribbean plate boundary, Dominican Republic. *Journal of Geophysical Research* 108 (B3), 2149. doi:10.1029/2001JB000442.
- Righter, K., Campbell, A.J., Humayun, M., Hervig, R.L., 2004. Partitioning of Ru, Rh, Pd, Re, Ir, and Au between Cr-bearing spinel, olivine, pyroxene and silicate melts. *Geochimica et Cosmochimica Acta* 68, 867–880.
- Roeder, P.L., Emslie, R.F., 1970. Olivine–liquid equilibrium. *Contributions to Mineralogy and Petrology* 29, 275–289.
- Sato, H., 1977. Nickel content of basaltic magmas: identification of primary magmas and a measure of the degree of olivine fractionation. *Lithos* 10, 113–120.
- Saumur, B.-M., Hattori, K.H., Guillot, S., 2010. Contrasting origins of serpentinites in the northern Dominican Republic. *Bulletin, Geological Society of America*. doi:10.1130/B26530.1.
- Seyler, M., Lorand, J.P., Dick, H.J.B., Drouin, M., 2007. Pervasive melt percolation reactions in ultra-depleted refractory harzburgites at the Mid-Atlantic Ridge, 15°20′N: ODP Hole 1274A. *Contributions to Mineralogy and Petrology* 153, 303–319.
- Simon, N.S.C., Irvine, G.J., Davies, G.R., Pearson, D.G., Carlson, R.W., 2003. The origin of garnet and clinopyroxene in “depleted” Kaapvaal peridotites. *Lithos* 71, 289–322.
- Sobolev, A.V., Hofmann, A.W., Sobolev, S.V., Nikogosian, I.K., 2005. An olivine-free mantle source of Hawaiian shield basalts. *Nature* 434, 590–597.
- Stern, R.J., Bloomer, S.H., 1992. Subduction zone infancy: examples from the Eocene Izu–Bonin–Mariana and Jurassic California arcs. *Bulletin, Geological Society of America* 104, 1621–1636.
- Suhr, G., Seck, H.A., Shimizu, N., Gunther, D., Jenner, G., 1998. Infiltration of refractory melts into the lowermost oceanic crust: evidence from dunite- and gabbro-hosted clinopyroxenes in the Bay of Islands Ophiolite. *Contributions to Mineralogy and Petrology* 131, 136–154.
- Suhr, G., Hellebrand, E., Johnson, K., Brunelli, D., 2008. Stacked gabbro units and intervening mantle: a detailed look at a section of IODP Leg 305, Hole U1309D. *Geochemistry Geophysics Geosystems* 9. doi:10.1029/2008GC002012.
- Syracuse, E.M., Abers, G.A., 2006. Global compilation of variations in slab depth beneath arc volcanoes and implications. *Geochemistry Geophysics Geosystems* 7. doi:10.1029/2005GC001045.
- Takahashi, E., 1986. Origin of basaltic magmas: implications from peridotite melting experiments and an olivine fractionation model. *Bulletin, Volcanology Society of Japan* 30, S17–S40 (in Japanese with English Abst.).
- Toplis, M.J., 2005. The thermodynamics of iron and magnesium partitioning between olivine and liquid: criteria for assessing and predicting equilibrium in natural and experimental systems. *Contributions to Mineralogy and Petrology* 149, 22–39.
- Tribuzio, R., Tiepolo, M., Fiameni, S., 2008. A mafic–ultramafic cumulate sequence derived from boninite-type melts (Niagara Icefalls, northern Victoria Land, Antarctica). *Contributions to Mineralogy and Petrology* 155, 619–633.
- Ulmer, P., Trommsdorff, V., 1995. Serpentine stability to mantle depths and subduction-related magmatism. *Science* 268, 858–861.
- Walker, D.A., Cameron, W.E., 1983. Boninite primary magmas: evidence from the Cape Vogel Peninsula, PNG. *Contributions to Mineralogy and Petrology* 83, 150–158.
- Wang, J., Hattori, K.H., Stern, C., 2008. Metasomatic origin of garnet orthopyroxenites in the subcontinental lithospheric mantle underlying Pali Aike volcanic field, southern South America. *Mineralogy and Petrology* 94, 243–258.
- Wilson, S.A., 1997. The collection, preparation, and testing of USGS reference material BCR-2, Columbia River, Basalt. U.S. Geological Survey Open-File Report 98.
- Zack, T., Rivers, T., Brumm, R., Kronz, A., 2004. Cold subduction of oceanic crust: implications from a lawsonite eclogite from the Dominican Republic. *European Journal of Mineralogy* 16, 909–916.
- Zhang, R.Y., Liou, G.J., Yang, J.S., Ye, K., 2003. Ultrahigh-pressure metamorphism in the forbidden zone: the Xugou garnet peridotite, Sulu terrane, eastern China. *Journal of Metamorphic Geology* 21, 539–550.